Editors' Suggestion

# Impact of mode regularization for quasinormal-mode perturbation theories

Sebastian Franke [1,2,*] Juanjuan Ren [2] and Stephen Hughes [2]

[1] *Technische Universität Berlin, Institut für Theoretische Physik, Nichtlineare Optik und Quantenelektronik, Hardenbergstraße 36, 10623 Berlin, Germany*

[2] *Department of Physics, Engineering Physics, and Astronomy, Queen's University, Kingston, Ontario, Canada K7L 3N6*

(Received 12 July 2023; accepted 8 August 2023; published 4 October 2023)

We give theoretical insight into the critical problem of a modified cavity mode of an open resonator that is subject to a perturbation outside its cavity region. We utilize the framework of quasinormal modes (QNMs), which are the natural mode solutions to the open boundary problem with complex eigenfrequencies. This requires a non-Hermitian mode theory, typically using just a few dominant QNMs for resonant cavities, which are important for solving a wide range of problems in classical and quantum optics, including cavity quantum electrodynamics. We first highlight a fundamental problem with currently adopted formulas using QNM perturbation theory, when perturbations are added outside the resonator structure and present a potential step for solving this problem, connected to a regularization of the QNMs. We show several calculations of the QNMs and regularized QNM theory for simple one-dimensional cavities as well as a practical three-dimensional cavity structure. We first concentrate on the illustrative case of a one-dimensional dielectric barrier, where analytical QNM solutions are possible. We study the change of the mode frequency as a function of distance between the cavity and another smaller barrier structure (forming the outside perturbation). The results obtained from a few QNM expansion are also compared with exact analytical solutions from a transfer matrix approach. We show explicitly how regularization prevents a problematic spatial divergence for QNM perturbations in the far-field region, though eventually higher-order effects and multimodes can also play a role in the full scattering solution, and retaining a pure discrete QNM picture becomes questionable in such situations since the input-output coupling ultimately involves reservoir modes. To investigate a more practical cavity example, we also show results for a full three-dimensional plasmonic resonator of arbitrary shape and complex dispersion and loss, which again displays the divergent nature of the first-order mode change predicted from regular QNM perturbation theory, and an exponentially damped behavior from our regularized QNM theory.

DOI: 10.1103/PhysRevA.108.043502

## I. INTRODUCTION

Perturbation theory of open resonators is an important topic in quantum and classical optics and has a variety of applications, such as the detection and sensing in the vicinity of a scattering object, including plasmonic or dielectric cavities [1–4]. The introduction of a perturbation into a resonator environment, e.g., a metallic tip, and its change of the permittivity values leads to a modification of the resonator's eigenmodes and frequencies. Alternative ways of perturbing the system include the deformation of the scattering object or the overall change of a material.

There are several theoretical techniques to describe these changes in the cavity mode properties, which are usually based on so-called modes of the universe [5–8], i.e., solutions of the Helmholtz equation with vanishing boundary conditions at $|\mathbf{r}| \to \infty$; or, in an approximate model, using so-called normal modes (NMs), which are solutions of the Helmholtz equation with fixed boundary conditions of the associated closed resonator [9]. While the former case involves a continuous set of normal modes, which are typically not tractable in a practical numerical simulation, the latter approach is only reliable for very high-quality factors ($Q$), namely, small radiation leakage of the resonators. Indeed, the cavity NM approach for cavities is only rigorous in the case of no loss since the eigenfrequencies are real, and is thus generally ambiguous for open cavities, even for high-$Q$ (quality factor) resonators.

In contrast to the high-$Q$ cavity normal mode, the usual modes-of-the-universe approaches [5–8] deal with simple dielectrics embedded in a much larger cavity system, where the continuous normal modes can be analytically computed. All modes vanish at the edge of the larger cavity system, and the problem is Hermitian. Unfortunately, such an approach is not practical for describing realistic three-dimensional (3D) resonators, where one computes the discrete dissipative cavity modes of the open resonator, with open boundary conditions, termed "quasinormal modes" (QNMs). Computation of the QNMs also enables one to easily include material loss and dispersion into the cavity region. In either case (modes of the universe or QNMs), one also must deal with the outside modes for a general solution, especially for field quantization. This was already made clear decades ago, e.g., in Ref. [6], where they write "Clearly, as a first step, one must relate the field operators inside and outside the cavity."

*sebastian.r.franke@gmail.com

 

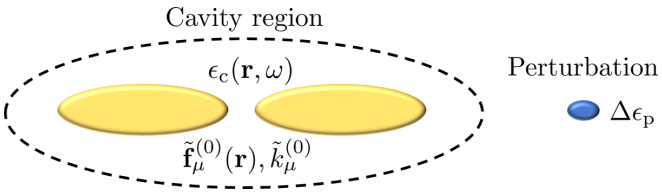


FIG. 1. Schematic of a resonator with permittivity $\epsilon_c(\mathbf{r}, \omega)$, perturbed by a small source with permittivity difference $\Delta\epsilon_p$ outside of the cavity region. The unperturbed cavity supports a set of QNMs with eigenfunctions $\tilde{\mathbf{f}}_\mu^{(0)}(\mathbf{r})$ and eigenwave numbers $\tilde{k}_\mu^{(0)} = \tilde{\omega}_\mu^{(0)}/c$, which form a complete representation of the field inside the cavity region.

A rigorous open resonator method not only allows one to investigate a change in the oscillation frequency of the cavity mode, but also a change of its spectral linewidth and temporal decay, which is not possible using a NM description (real frequencies). The general eigensolutions to this open cavity problem are QNMs [4,10–15], which have complex mode frequencies. Moreover, the QNMs can also be formulated for general dispersive and absorptive cavities, where simpler approaches, like the modes-of-the-universe description (in its usual form), cannot be used anymore [16].

Various QNM and open-cavity modes techniques have been used quite extensively in recent years, presenting a powerful and successful description of light-matter interactions close or within the resonator object [4,13,14,17–21]. Such approaches also include a generalization of well-known perturbation theories, which have been typically described on the basis of NMs. In particular, this allows one to describe perturbation inside an open cavity [22,23] or even close to an open-cavity region for near-field optics in both linear [24,25] and nonlinear regimes [26].

However, the spatial divergence of QNMs prevents one to describing phenomena that happen far outside the resonator region, as depicted in Fig. 1 (which is, of course, also problem dependent). The divergence stems from the open boundary conditions in combination with complex eigenfrequencies with a negative imaginary part (assuming lossy media [27]). Importantly, this is not just a particular problem of QNMs, but is an intrinsic property of all open-cavity systems that are not treated phenomenologically as closed systems with dissipation added *ad hoc*. Apart from some very brief discussions about this potential problem of using QNMs for perturbation theory integrals, to our knowledge this "problem" has not been addressed in the literature. However, since it is the most natural way of using cavity-mode theory, it is clearly a very important problem to try and solve.

While much progress has been made into rigorously fixing the divergent behavior of QNMs for formulating a well-defined Purcell factor [28,29] (i.e., the enhanced or suppressed spontaneous emission rate of a dipole emitter), general far-field quantities [30], and a rigorous QNM quantization method [31–33]; not much has been done in terms of a generalized perturbation theory. Similar to using a closed-cavity approach, QNM theories also start to become invalid in this regime, and are generally ambiguous for any perturbation *outside* the cavity structure. In a more general view, the same conceptional problem applies to practical cavity circuits, such as waveguide-cavity systems, where two well-separated open and lossy resonators may interact through a waveguide structure (involving the propagating waveguide modes). As recognized and discussed recently [34], this is a promising structure for setting up a quantum network of several quantum emitters attached to the cavities [35].

In this work, we highlight general problems with QNM perturbation theory and apply mode regularization methods to fix the divergent behavior as a function of distance. Although we concentrate on two specific examples in this work, the regularization methods are completely general and they have already been successfully applied in other light-matter interaction problems, such as the calculation of a Purcell factor for an emitter-cavity system with a large separation (i.e., the dipole is in the region where the QNM starts to spatially diverge) [28].

In Sec. II, we introduce some background QNM theory, and discuss a Green function expansion in terms of QNMs and regularized QNMs. In Sec. IV, we present the perturbation theory for QNMs and highlight the inherent modeling problem with adding perturbations outside the cavity region, which renders current perturbation approaches ambiguous in general. In Sec. V, we present several applications for the one-dimensional case, including the calculation of the local density of states (LDOS) for a single-barrier cavity as well as the calculation of eigenfrequencies of a double-barrier cavity system, using an exact transfer matrix approach and a first-order perturbation theory. Additionally, we investigate the eigenfrequencies of a fully three-dimensional cavity perturbed by a small spherical particle. In Sec. VI, we then discuss the whole problem from different views, and also elaborate on a possible alternative representation of the QNM Green function (which is nondiagonal in the QNM expansion). Finally, in Sec. VII, we give our conclusions.

In addition, we present several Appendixes, including the equivalence of different regularized QNM approaches, the derivation of two Green identities, and details of the contour integration in connection with a nondiagonal form of a QNM Green function.

## II. QUASINORMAL-MODE THEORY

In this section, we present some important background theory and properties of QNMs, formulated for QNM perturbation theory.

We first consider the isolated open-cavity structure embedded in a lossless background. The unperturbed QNM eigenfunctions $\tilde{\mathbf{f}}_\mu^{(0)}$ are solutions to the Helmholtz equation

$$\left\{\nabla\times\nabla\times - \left[\tilde{k}_\mu^{(0)}\right]^2 \epsilon_c(\mathbf{r}, \tilde{\omega}_\mu^{(0)})\right\}\tilde{\mathbf{f}}_\mu^{(0)}(\mathbf{r}) = 0, \tag{1}$$

together with open boundary conditions, i.e., the Silver-Müller radiation conditions

$$\frac{\mathbf{r}}{|\mathbf{r}|}\times\nabla\times\tilde{\mathbf{f}}_\mu^{(0)}(\mathbf{r}) \to in_B\tilde{k}_\mu^{(0)}\tilde{\mathbf{f}}_\mu^{(0)}(\mathbf{r}), \tag{2}$$

which are asymptotic relations for $|\mathbf{r}| \to \infty$. Here, $\tilde{k}_\mu^{(0)} = \tilde{\omega}_\mu^{(0)}/c$, where $c$ is the vacuum speed of light, and $\tilde{\omega}_\mu^{(0)} = \omega_\mu^{(0)} - i\gamma_\mu^{(0)}$ is the unperturbed QNM eigenfrequency, which

is a complex number due to the open boundary conditions. In the following, we use the term "eigenfrequency" for $\tilde{k}_\mu$ and $\tilde{\omega}_\mu$ interchangeably (implicitly setting $c = 1$).

The associated QNM resonance has a real part of the frequency $\omega_\mu^{(0)}$ and a half-width at half-maximum $\gamma_\mu^{(0)}$ (which comes from the imaginary part of the eigenfrequency, where $\gamma_\mu^{(0)} = \omega_\mu^{(0)}/[2Q_\mu^{(0)}]$). Furthermore, $\epsilon_c(\mathbf{r}, \tilde{\omega}_\mu^{(0)})$ is the analytical continuation of the complex-valued permittivity function $\epsilon_c(\mathbf{r}, \omega)$, that describes a spatial-inhomogeneous and (possibly) dispersive resonator geometry embedded in a background medium, with constant and real-valued refractive index $n_B$, as visualized in Fig. 1 (shown without an additional perturbation).

When properly normalized, the QNMs can be used as a basis to expand the transverse part of the Green function $\mathbf{G}(\mathbf{r}, \mathbf{r}_0, \omega)$, which describes the light propagation from a source point $\mathbf{r}_0$ to $\mathbf{r}$, and is formally defined via the Helmholtz equation

$$\left[\boldsymbol{\nabla} \times \boldsymbol{\nabla} \times -k_0^2 \epsilon_c(\mathbf{r}, \omega)\right] \mathbf{G}(\mathbf{r}, \mathbf{r}_0, \omega) = k_0^2 \delta(\mathbf{r} - \mathbf{r}_0), \tag{3}$$

together with suitable radiation conditions, namely, Eq. (2), for real-valued frequencies $\omega$ and $k_0 = \omega/c$. The resulting QNM expanded form of the transverse part of the Green function $\mathbf{G}^\perp(\mathbf{r}, \mathbf{r}_0, \omega)$ for spatial positions inside the resonator geometry is

$$\mathbf{G}^\perp(\mathbf{r}, \mathbf{r}_0, \omega) = \sum_\mu A_\mu^{(0)}(\omega) \tilde{\mathbf{f}}_\mu^{(0)}(\mathbf{r}) \tilde{\mathbf{f}}_\mu^{(0)}(\mathbf{r}_0), \tag{4}$$

with $A_\mu^{(0)}(\omega) = \omega/[2(\tilde{\omega}_\mu^{(0)} - \omega)]$, and in general, the sum runs over all $\mu = 0, \pm 1, \pm 2, \ldots$ with the imposed ordering $0 < \omega_1 < \omega_2 < \cdots$ and symmetry properties $\tilde{\mathbf{f}}_{-\mu}^{(0)} = \tilde{\mathbf{f}}_\mu^{(0)*}$, as well as $\tilde{\omega}_{-\mu}^{(0)} = -\tilde{\omega}_\mu^{(0)*}$. We note that although the full set of modes including the so-called "zero mode" [36] ($\mu = 0$) are required for general completeness of QNMs, only a few QNMs with $\mu > 0$ are needed in practical situations of classical and quantum optics. Indeed, this is what makes a QNM approach so powerful.

One of the drastic consequences of the open boundary conditions is that the QNMs spatially diverge for far-field positions, and completeness can only be achieved within the resonator region. Strictly speaking, this is correct only for resonator embedded in a spatial-homogeneous background and completeness was only proven explicitly for certain resonator types, e.g., of spherical shape or one-dimensional cavities [11,16,37]. In general, for the common case of resonators lying on substrates, branch cuts exist and the QNM basis is incomplete (cf. Refs. [4,15] and references therein). However, completeness is restored in advanced theories using additional numerical modes (see Refs. [38,39], for instance). Since completeness is required for an eigenfunction expansion of the Green function, Eq. (4) must be adapted for positions in the background region. Otherwise, this would prevent one from using the QNM expansion as a basis to calculate any spatial overlap outside of the cavity region, which is necessary to calculate frequency changes for perturbations located in the background region.

It is noteworthy that, for the case of purely amplifying media and where gain overcompensates the radiative loss, the imaginary part of the QNM eigenfrequencies would change the sign of $\gamma_\mu$. As a consequence, the resulting *gain* QNMs [27] would be spatially damped in the far field, and the divergence would instead appear in the time domain. However, treating such cases on the level of linear amplification would not be consistent with the causality relation or (in frequency space) the Kramers-Kronig relations of $\mathbf{G}(\mathbf{r}, \mathbf{r}_0, \omega)$, which is necessary to formulate a QNM quantization formalism [40,41].

## III. QUASINORMAL-MODE REGULARIZATION

As an option to circumvent or resolve this QNM divergence problem, one can introduce a *regularization* procedure of the QNMs by exploiting an integral form of the Green function or the field equivalence principle, where the former is related to the well-known (classical) Dyson equation. Such regularization not only prevents unphysical behavior of important classical quantities, such as an increasing enhancement of the spontaneous emission in the far field of a metallic antenna [28,29], but it is also required to properly predict the radiative dissipation in a quantized QNM theory [31–33].

It is important to note that this regularization is not just a heuristic fix for diverging QNMs (which is sometimes misunderstood in the literature); the regularized QNM functions we use below are rigorously defined using only fundamental Green's identities as well as the completeness of the QNMs *inside* the resonator volume (or at the resonator boundary). These QNM functions carry over the characteristics of the (infinitely extended) background medium through a real continuous frequency $\omega$ for each discrete QNM, which is physically intuitive and in line with system-bath and input-output theories, where they can be interpreted as reservoir modes. We elaborate more on that point later. Indeed, not using these regularized QNMs would be problematic for a certain class of problems if one wants to keep the theory within the framework of a few mode description, a concept already well known in open-system quantum optics.

Next, we elaborate and give further insights on the different QNM regularization procedures. All the methods exploit the assumed completeness of the QNMs, and as a consequence of the this completeness, the full (transverse) electric field $\mathbf{E}(\mathbf{r}, t)$ (of the unperturbed structure) at position $\mathbf{r}$ in the cavity region can be represented as

$$\mathbf{E}(\mathbf{r}, t) = \sum_\mu a_\mu^{(0)}(t) \tilde{\mathbf{f}}_\mu^{(0)}(\mathbf{r}), \tag{5}$$

where $a_\mu^{(0)}(t) = e^{-i\tilde{\omega}_\mu^{(0)} t} a_\mu^{(0)}(t = 0)$ is the harmonic solution to the temporal part of the wave equations.

First, we can define a regularized QNM by formulating the analog of Eq. (1) for the Fourier transform of $\mathbf{E}(\mathbf{r}, t)$, namely, using $\boldsymbol{\mathcal{E}}(\mathbf{r}, \omega)$ in a scattering problem. This leads to the following solution:

$$\begin{aligned} \boldsymbol{\mathcal{E}}(\mathbf{R}, \omega) = \boldsymbol{\mathcal{E}}_{\text{hom}}(\mathbf{R}, \omega) \\ + \int d^3 r \, \Delta\epsilon_c(\mathbf{r}, \omega) \mathbf{G}_B(\mathbf{R}, \mathbf{r}, \omega) \cdot \boldsymbol{\mathcal{E}}(\mathbf{r}, \omega), \end{aligned} \tag{6}$$

where $\mathbf{G}_B(\mathbf{R}, \mathbf{r}, \omega)$ is the background Green function, obtained from the solution of Eq. (3) with $\epsilon_c(\mathbf{r}, \omega) \to n_B^2$, and $\Delta\epsilon_c(\mathbf{r}, \omega) = \epsilon_c(\mathbf{r}, \omega) - n_B^2$ restricts the spatial integral to the

cavity volume. Since we demand consistency with the Silver-Müller radiations conditions, the only possible homogeneous solution is $\boldsymbol{\mathcal{E}}_{\rm hom}(\mathbf{R},\omega)=\mathbf{0}$.

Using the completeness relation of the QNMs *inside* the resonator volume, we can rewrite Eq. (6) as

$$\boldsymbol{\mathcal{E}}(\mathbf{R},\omega)=\sum_{\mu} a_{\mu}^{(0)}(\omega)\tilde{\mathbf{F}}_{\mu}^{(0)}(\mathbf{R},\omega), \tag{7}$$

where

$$\tilde{\mathbf{F}}_{\mu}^{(0)}(\mathbf{R},\omega)=\int d^3r\,\Delta\epsilon_{\rm c}(\mathbf{r},\omega)\mathbf{G}_{\rm B}(\mathbf{R},\mathbf{r},\omega)\cdot\tilde{\mathbf{f}}_{\mu}^{(0)}(\mathbf{r}) \tag{8}$$

is a function of *real frequency* $\omega$. The QNM eigenfunctions $\tilde{\mathbf{f}}_{\mu}^{(0)}(\mathbf{r})$ are fundamentally connected to the above regularized QNM functions via analytical continuation of $\omega$ into the complex area, i.e., $\tilde{\mathbf{F}}_{\mu}^{(0)}(\mathbf{r},\tilde{\omega}_{\mu}^{(0)})=\tilde{\mathbf{f}}_{\mu}^{(0)}(\mathbf{r})$; consequently, we also refer to $\tilde{\mathbf{F}}_{\mu}$ as a "mode," but one which is now regularized. Note that in the one-dimensional case, for a cavity with boundaries $x=a,b$, there is an interesting relation between $\tilde{F}_{\mu}(x>b,\omega_{\mu})$ and $\tilde{F}_{\mu}(x>b,\tilde{\omega}_{\mu})$, namely,

$$\tilde{F}_{\mu}(x,\omega_{\mu})=e^{-\gamma_{\mu}n_{\rm B}(x-b)/c}\,\tilde{F}_{\mu}(x,\tilde{\omega}_{\mu}), \tag{9}$$

which will be discussed in more detail in Sec. V.

In the more general three-dimensional case, a similar relation only exists for $|\mathbf{r}|\to\infty$, through

$$\tilde{\mathbf{F}}_{\mu}(\mathbf{r},\omega_{\mu})\to e^{-\gamma_{\mu}n_{\rm B}|\mathbf{r}|/c}\tilde{\mathbf{F}}_{\mu}(\mathbf{r},\tilde{\omega}_{\mu}), \tag{10}$$

which is still an approximate relation since $\tilde{\mathbf{F}}_{\mu}(\mathbf{r},\omega)$ contains additional $\omega$-dependent terms, that are not part of the exponential function. If such a relation would exist for all positions outside the resonator, one could significantly improve the numerical calculations, as one would only need the QNM for outside positions multiplied by $e^{-\gamma_{\mu}n_{\rm B}|\mathbf{r}|/c}$.

Exploiting a form of Green's theorem, together with the Helmholtz equation of $\boldsymbol{\mathcal{E}}(\mathbf{r},\omega)$ and $\mathbf{G}_{\rm B}(\mathbf{R},\mathbf{r},\omega)$, one can find an alternative expression for the Fourier transform $\boldsymbol{\mathcal{E}}(\mathbf{R},\omega)$ outside the resonator region (cf. Appendix A for details):

$$\boldsymbol{\mathcal{E}}(\mathbf{R},\omega)=\sum_{\mu} a_{\mu}^{(0)}(\omega)\tilde{\mathbf{F}}_{\mu}^{\prime(0)}(\mathbf{R},\omega), \tag{11}$$

with

$$\begin{aligned}\tilde{\mathbf{F}}_{\mu}^{\prime(0)}(\mathbf{R},\omega)=&\frac{c^2}{\omega^2}\int_{\mathcal{S}'}dA_{\mathbf{s}}\mathbf{G}_{\rm B}(\mathbf{R},\mathbf{s},\omega)\cdot\left[\mathbf{n}\times\boldsymbol{\nabla}\times\tilde{\mathbf{f}}_{\mu}^{(0)}(\mathbf{s})\right]\\&-\frac{c^2}{\omega^2}\int_{\mathcal{S}'}dA_{\mathbf{s}}[\mathbf{n}\times\boldsymbol{\nabla}\times\mathbf{G}_{\rm B}(\mathbf{s},\mathbf{R},\omega)]^{\rm t}\cdot\tilde{\mathbf{f}}_{\mu}^{(0)}(\mathbf{s}),\end{aligned} \tag{12}$$

where $\mathcal{S}'$ is a surface that surrounds the scattering volume defined by $\Delta\epsilon_{\rm c}(\mathbf{r},\omega)$, $\mathbf{R}$ is located outside of $\mathcal{S}'$ and the superscript "t" denotes the transpose. We note that an implicit condition for this form assumes that the QNMs are a valid representation for the electric field at $\mathcal{S}'$, and thus one is usually limited to surfaces very close to the scattering volume. We further note that this result can also be obtained via the field equivalence principle [42], or similarly by a near-field to far-field transformation technique [33].

Furthermore, choosing $\mathcal{S}'$ as the surface of the scattering volume leads to the equivalence of Eqs. (11) and (7), as shown in Appendix A. However, these representations are not identical in a few-QNM approximation since different parts of the QNM set will contribute differently to the overall completeness at $\mathcal{S}'$ and in $V$ (scattering volume). Nevertheless, as shown in Ref. [33], both regularization methods behave similarly for far-field positions, i.e., for $|\mathbf{R}|\gg\lambda_{\mu}^{(0)}$, where $\lambda_{\mu}^{(0)}=2\pi c/(n_{\rm B}\omega_{\mu}^{(0)})$ is the associated wavelength of the unperturbed QNM.

We emphasize that while these techniques are well known in electromagnetic theories involving scattering sources, they do not follow a "mode" solution, which solves the *source-free problem*. Thus, mixing these concepts is a highly nontrivial step, which is for instance also required in quantum mode theories (such as open-system cavity quantum electrodynamics), where the decay and dissipation is modeled through a reservoir with continuous degrees of freedom. These degrees of freedom are precisely captured by $\omega$ in $\tilde{\mathbf{F}}_{\mu}(\mathbf{r},\omega)$.

## IV. PERTURBATION THEORY OF OPEN RESONATORS

In Sec. II, we discussed the unperturbed problem with a single cavity supporting a set of QNMs with eigenfunctions and eigenfrequencies $\{\tilde{\mathbf{f}}_{\mu}^{(0)},\tilde{\omega}_{\mu}^{(0)}\}$. When adding another scattering object with volume $V$, yielding the permittivity $\epsilon_{\rm p}(\mathbf{r},\omega)=\epsilon_{\rm B}+\Delta\epsilon_{\rm p}(\mathbf{r},\omega)$, such as a molecule or detector object outside the cavity structures, the permittivity function changes to $\epsilon(\mathbf{r},\omega)=\epsilon_{\rm c}(\mathbf{r},\omega)+\Delta\epsilon_{\rm p}(\mathbf{r},\omega)$. One could again solve the source-free Helmholtz equation by replacing $\epsilon_{\rm c}\to\epsilon$ to obtain the full QNM eigenfunctions and eigenfrequencies $\{\tilde{\mathbf{f}}_{\mu},\tilde{\omega}_{\mu}\}$. However, usually, this is a very numerically demanding task, especially for three-dimensional structures. It also offers no analytical insight.

In this section, we will discuss the possibility to utilize the regularization of QNMs for formulating a QNM framework, where the cavity-perturbation setup, as visualized in Fig. 1, could be tackled within the initial unperturbed QNM basis.

First, we will analyze the problem that appears when simply using $\tilde{\mathbf{f}}_{\mu}^{(0)}(\mathbf{r})$. Adopting the one-dimensional time-independent perturbation technique from Refs. [16,43], for a general three-dimensional system, a first-order correction to $\tilde{k}_{\mu}^{(0)}$ can be calculated in the general dispersive case as

$$\tilde{k}_{\mu}^{(1)}=-\frac{\tilde{k}_{\mu}^{(0)}}{2}\int d^3r\,\Delta\epsilon_{\rm p}(\mathbf{r},\tilde{\omega}_{\mu}^{(0)})\tilde{\mathbf{f}}_{\mu}^{(0)}(\mathbf{r})\cdot\tilde{\mathbf{f}}_{\mu}^{(0)}(\mathbf{r}). \tag{13}$$

To show the conceptional failure of the QNMs, in a very simple and intuitive way, we can move a pointlike perturbation to the very far field at $\mathbf{X}_{\rm far}$ and then derive the first-order perturbation modification (assuming a dispersionless permittivity for the perturbation, with volume $V_{\rm p}$):

$$\begin{aligned}\tilde{k}_{\mu}^{(1)}&=-\frac{\tilde{k}_{\mu}^{(0)}}{2}V_{\rm p}\Delta\epsilon_{\rm p}\,\tilde{\mathbf{f}}_{\mu}^{(0)}(\mathbf{X}_{\rm far})\cdot\tilde{\mathbf{f}}_{\mu}^{(0)}(\mathbf{X}_{\rm far})\\&\propto-\frac{\tilde{k}_{\mu}^{(0)}}{2}V_{\rm p}\Delta\epsilon_{\rm p}\,e^{in_{\rm B}\omega_{\mu}^{(0)}|\mathbf{X}_{\rm far}|/c}e^{n_{\rm B}\gamma_{\mu}^{(0)}|\mathbf{X}_{\rm far}|/c},\end{aligned} \tag{14}$$

whose form is a consequence of the Silver-Müller radiation conditions. Although this is the currently accepted form of QNM perturbation theories, it clearly diverges for $|\mathbf{X}_{\rm far}|\to\infty$.

One heuristic approach to fix this divergence problem would be to utilize the regularization of the QNMs *outside*

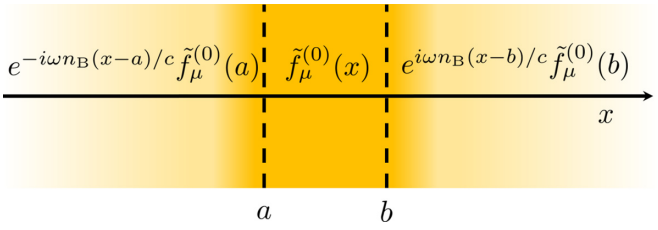


FIG. 2. Schematic of a one-dimensional cavity in the $x$ direction, with a visualization of the regularization procedure using the surface form. The QNM eigenfunctions $\tilde{f}_\mu(x)$ form a complete set inside the resonator region $x \in [a, b]$, and propagate out as plane waves through the outgoing boundary conditions (16). The regularization ensures a convergent outgoing field with a real frequency $\omega$, from which one can associate a convergent regularized mode by taking $\omega \to \omega_\mu$ at the real part of the complex QNM eigenfrequencies.

the resonator region (introduced in Sec. II), thus replacing $\tilde{\mathbf{f}}_\mu^{(0)}$ by $\tilde{\mathbf{F}}_\mu^{(0)}$ for positions $\mathbf{r}$ outside the resonator. Note that taking a resonant approximation $\tilde{\mathbf{F}}_\mu^{(0)}(\mathbf{r}, \omega) \to \tilde{\mathbf{F}}_\mu^{(0)}(\mathbf{r}, \omega_\mu^{(0)})$, is needed in this case since a $\omega$-dependent frequency change is not in the spirit of with a modal picture. In this way, the divergent behavior of $\tilde{\mathbf{f}}_\mu^{(0)}(\mathbf{r})$ could be circumvented, as $\tilde{\mathbf{F}}_\mu^{(0)}(\mathbf{r}, \omega_\mu^{(0)})$ takes on a real frequency value. However, as will be shown in Sec. V, this simple replacement is not sufficient to cover all effects that can modify the initial QNM parameters. Nevertheless, at least the spatial divergence from the usual QNM approach is can be prevented.

## V. APPLICATIONS

In this section, we will next show some specific examples to demonstrate the impact of the regularization technique on QNM perturbation theory.

### A. Single-barrier problem

#### 1. *Quasinormal modes of a single barrier*

We first study the problem of an unperturbed single cavity in the form of a single barrier with constant refractive index, spanning from $x = a$ to $b$, as sketched in Fig. 2. We shall denote the length of the cavity as $L$ and the refractive index of the resonator as $n_R$.

For the simple case of a single barrier, the QNM eigenfrequencies can be calculated via

$$n_R \tilde{k}_\mu^{(0)} L = \mu\pi + \frac{i}{2} \ln\left[\frac{(n_R - n_B)^2}{(n_R + n_B)^2}\right], \tag{15}$$

where we made use of the outgoing boundary conditions, which read explicitly as

$$\partial_x \tilde{f}_\mu^{(0)}(x)\big|_{x\nearrow a} = -i\tilde{\omega}_\mu n_B/c \tilde{f}_\mu^{(0)}(a), \tag{16a}$$

$$\partial_x \tilde{f}_\mu^{(0)}(x)\big|_{x\searrow b} = i\tilde{\omega}_\mu n_B/c \tilde{f}_\mu^{(0)}(b). \tag{16b}$$

Interestingly, we observe that the "zero mode" ($\mu = 0$) is purely imaginary and vanishes in the lossless limit.

In the following, we choose the refractive indices $n_B = 1$ and $n_R = 2\pi$ for the background and resonator, respectively. For these parameters, we obtain the $\mu$-independent quality factor $Q \approx 20$, resulting in an intermediate cavity finesse. We note that there are realistic examples with even lower-$Q$ factor, such as the plasmonic resonator (which is commonly used in optical sensing technologies), where we expect an even more drastic failure from the use of a complex QNM for positions outside the resonator region.

The associated QNM eigenfunctions, which are normalized, can be derived as (cf. Ref. [15])

$$\tilde{f}_\mu^{(0)}(x) = \frac{e^{in_R \tilde{k}_\mu^{(0)}(x-x_0)} + (-1)^\mu e^{-in_R \tilde{k}_\mu^{(0)}(x-x_0)}}{\sqrt{(-1)^\mu 2L\, n_R}}, \tag{17}$$

within the cavity region with center $x = x_0$. For positions outside the barrier, we have

$$\tilde{f}_\mu^{(0)}(x > b) = e^{-i\tilde{\omega}_\mu n_B/c(x-b)} \tilde{f}_\mu^{(0)}(b), \tag{18a}$$

$$\tilde{f}_\mu^{(0)}(x < a) = e^{-i\tilde{\omega}_\mu n_B/c(a-x)} \tilde{f}_\mu^{(0)}(a). \tag{18b}$$

In one spatial dimension, one can formulate a generalized norm integral as

$$\langle\langle \tilde{f}_\mu^{(0)} | \tilde{f}_\mu^{(0)} \rangle\rangle = \int_a^b dx\, \epsilon(x) \big[\tilde{f}_\mu^{(0)}(x)\big]^2 + i\frac{n_B c}{2\tilde{\omega}_\mu} \big\{\big[\tilde{f}_\mu^{(0)}(a)\big]^2 + \big[\tilde{f}_\mu^{(0)}(b)\big]^2\big\}, \tag{19}$$

where we have defined $a = x_0 - L/2$, $b = x_0 + L/2$. For a detailed derivation of a limiting case of one open boundary, see Ref. [11]. For a constant permittivity $\epsilon(x) = n_R^2$ in $[a, b]$, Eq. (19) reduces to $\langle\langle \tilde{f}_\mu^{(0)} | \tilde{f}_\mu^{(0)} \rangle\rangle = 1$, when using the solution from Eq. (17). In the following, we will not specify the length $L$ of the cavity, as it simply sets the scale of the cavity problem.

#### 2. *Mode regularization and the local density of states*

For the one-dimensional analysis, the special case of Eq. (12) gives

$$\tilde{F}_\mu'^{(0)}(x, \omega) = e^{in_B k_0 (x-b)} \tilde{f}_\mu^{(0)}(b) \tag{20}$$

for $x > b$, and

$$\tilde{F}_\mu'^{(0)}(x, \omega) = e^{-in_B k_0 (x-a)} \tilde{f}_\mu^{(0)}(a) \tag{21}$$

for $x < a$. These solutions are right- and left-propagating plane waves with continuity conditions at the boundary, i.e., $\tilde{F}_\mu'^{(0)}(x, \omega)|_{x\nearrow a} = \tilde{f}_\mu^{(0)}(a)$ and $\tilde{F}_\mu'^{(0)}(x, \omega)|_{x\searrow b} = \tilde{f}_\mu^{(0)}(b)$ independent of $\omega$. On the other hand, the regularized QNM from the volume integral representation (8) would simplify to

$$\tilde{F}_\mu^{(0)}(x, \omega) = \frac{ik_0}{2n_B} e^{in_B k_0 x} \int_a^b ds\, \Delta\epsilon(s) e^{-in_B k_0 s} \tilde{f}_\mu^{(0)}(s) \tag{22}$$

for $x > b$, and

$$\tilde{F}_\mu^{(0)}(x, \omega) = \frac{ik_0}{2n_B} e^{-in_B k_0 x} \int_a^b ds\, \Delta\epsilon(s) e^{in_B k_0 s} \tilde{f}_\mu^{(0)}(s) \tag{23}$$

for $x < a$. In contrast to $\tilde{F}_\mu'^{(0)}(x, \omega)$ (obtained as a one-dimensional limit from the surface integral representation), $\tilde{F}_\mu^{(0)}(x, \omega)$ (obtained as a one-dimensional limit from the volume integral representation) does not fulfill the continuity conditions. However, again we emphasize that the full electric

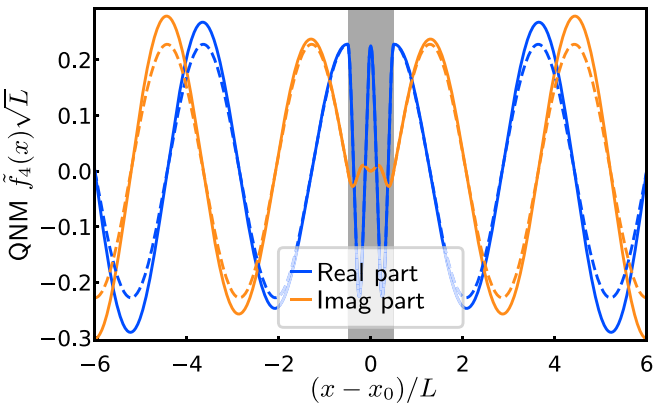


FIG. 3. Real [blue (dark)] and imaginary [orange (light)] parts of normalized QNM $\tilde{f}_\mu^{(0)}(x)$ ($\mu = 4$) for the (unperturbed) single-barrier cavity with center $x_0$, length $L$, background refractive index $n_B = 1$, and slab index $n_R = 2\pi$, using Eqs. (17) and (18). The gray dashed area marks the cavity region. The corresponding quality factor is $Q^{(0)} \approx 20$ (and is identical for all $\mu$). The dashed lines reflect the result from a regularization outside the resonator within a pole approximation at $k = \mathrm{Re}[\tilde{k}_4]$, i.e., $\tilde{F}_\mu'^{(0)}(x, \omega_\mu)$ ($\mu = 4$), using Eqs. (20) and (21).

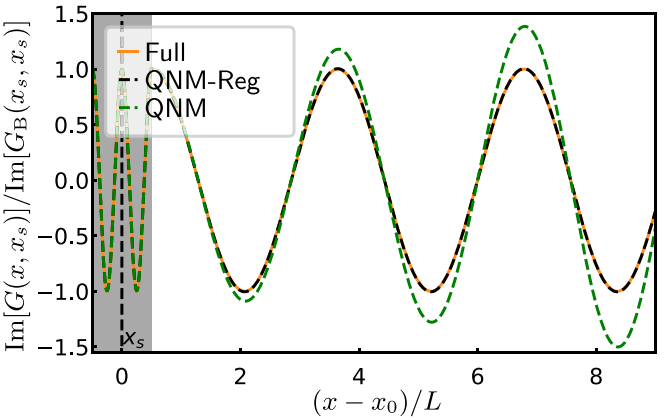


FIG. 4. Imaginary part of the single-barrier propagators $G(x, x_s, k = \mathrm{Re}[\tilde{k}_4])$ normalized by $\mathrm{Im}[G_B(x_s, x_s)] = 1/(2n_B\mathrm{Re}[\tilde{k}_4])$ with the source point $x_s = x_0$ (located in the center of the cavity) using the exact Green function ansatz [solid orange curve, see legend, Eq. (26)], the single QNM approximation [green dashed curve, Eq. (24) with $\mu = 4$], and the single QNM approximation with regularization [black dashed curve, Eq. (25), with $\mu = 4$]. Note that $n_R = 2\pi$, which results in a quality factor of $Q \approx 20$.

field (including all QNMs) is still identical within both representations (cf. Appendix A). In the following we will use the surface integral representation in the few-QNM approximation.

In Fig. 3, we show precisely the difference between the complex QNM [Eqs. (17) and (18)] and the regularized QNM [Eqs. (20) and (21)] for the described exemplary single-barrier cavity. By construction, the regularized QNMs are a combination of the complex QNM inside the cavity region and represent plane waves with the real frequency $\omega_\mu$ outside the single barrier.

As a first test of the regularized QNM, we look at the imaginary part of the Green function, which is important for many calculations in optics and nanophotonics, e.g., the Purcell factor, which describes the enhancement or suppression of the spontaneous emission of an emitter placed close to the resonator (which uses the Green function with equal space arguments).

In terms of a QNM expansion, the Green function $G(x, x_s, \omega)$ can be written as

$$G_{\mathrm{QNM}}(x, x_s, \omega) = \sum_\mu A_\mu(\omega)\tilde{f}_\mu(x)\tilde{f}_\mu(x_s) \tag{24}$$

for the complex QNM form (without regularization), and

$$G_{\mathrm{QNM}}^{\mathrm{reg}}(x, x_s, \omega) = \sum_\mu A_\mu(\omega)\tilde{F}_\mu(x, \omega_\mu)\tilde{f}_\mu(x_s) \tag{25}$$

for the regularized QNM form, where $x_s$ is located inside the resonator region $[a, b]$, $x > b$, and $A_\mu = \omega/[2(\tilde{\omega}_\mu - \omega)]$. In this simple geometry sample, we can compare with the exact solution, where for $x_s \in [a, b]$ and $x > b$, then

$$G_{\mathrm{exact}}(x, x_s, \omega) = A(x_s, \omega)e^{in_B kx} = A(x_s, \omega)e^{in_B\omega x/c}, \tag{26}$$

where

$$A(x_s, \omega) = -\frac{i}{2n_R k}e^{-ik(n_R+n_B)(b-a)/2}(1+\beta) \times \frac{e^{ikn_R(b-a+x_s)} + \beta e^{-ikn_R(b-a)}}{e^{ikn_R(b-a)} - \beta^2 e^{-ikn_R(b-a)}}, \tag{27}$$

with $\beta = (n_R - n_B)/(n_R + n_B)$.

We next concentrate on a single QNM expansion, using the QNM $\mu = 4$ and the parameters described in Sec. V A 1. As shown in Fig. 4, the results using the regularized QNM [Eq. (25)] are in very good agreement with the full analytical Green function solution on the basis of a plane-wave expansion [without any approximation, Eq. (26)]. In contrast, using the expansion with $\tilde{f}_4$ [Eq. (24)] would lead to a divergent behavior, as shown by the green dashed curve in Fig. 4, as expected. This example clearly highlights the need to perform mode regularization in general, if adopting a few-mode expansion approach (which is a requirement for many applications in quantum optics). One should note here that while the imaginary part of the Green function within a single QNM approximation is in excellent agreement with the full analytical solution for the single-barrier cavity, this is not the case for the real part, where (in the current example) one needs $N > 100$ QNMs to obtain the same level of agreement.

### B. Double-barrier problem

After discussing the single-barrier problem in terms of of QNMs and regularized QNMs, we will now turn to the double-barrier problem, as depicted in Fig. 5. We will concentrate on the changes that the second barrier induces to the eigenfrequencies of the single-barrier cavity. This will be tackled in two different ways: (i) we will give a numerically exact solution, utilizing a transfer matrix approach, which can be used to derive the QNM poles directly or to extract them from the exact transmission (or reflection) coefficient (which

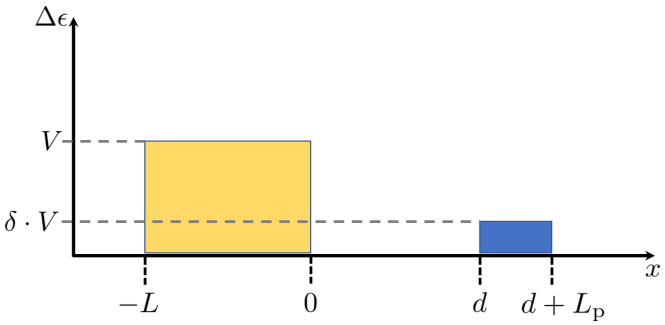


FIG. 5. Permittivity difference $\Delta\epsilon(x) = \epsilon(x) - \epsilon_B$ for the resonator-perturbation setup in one spatial dimension as function of $x$. A resonator with boundaries $x = -L, 0$ and permittivity difference $\Delta\epsilon_c(x) = V = 4\pi^2 - 1$ is embedded in a homogeneous background medium with refractive index $n_B = 1$, including a perturbation with permittivity difference $\Delta\epsilon_p = \delta V$, with length $L_p$ and distance $d$ from the cavity.

obviously has no mode approximations); (ii) we will apply the adapted perturbation theory to the geometry of interest, where for spatial coordinates outside the first barrier $\tilde{f}_\mu^{(0)}$ is replaced by $\tilde{F}_\mu'^{(0)}$.

#### 1. Direct solution from a transfer matrix approach

Here, we discuss an exact scattering treatment to obtain the eigenfrequencies of the double-barrier problem, by means of a transfer matrix approach. For this method, we adopt the approach of calculating the transfer matrix [44,45]. Note that completeness of the QNMs in a region within the outermost discontinuities in $n(x) = \sqrt{\epsilon(x)}$ has been shown elsewhere, a thorough proof can be found in Ref. [44]. Generally, in the spatial interval $[a_{j-1}, a_j]$ [which marks the positions of the discontinuities in $n(x)$], we define the solution to the one-dimensional Helmholtz equation as forward and backward traveling waves, from

$$\mathcal{E}_j(x,\omega) = A_j e^{ik_j x} + B_j e^{-ik_j x}, \tag{28}$$

with $k_j = n_j\omega/c$ [and $n(x)$ is piecewise constant], which are connected via boundary conditions

$$\mathcal{E}_j(a_j,\omega) = \mathcal{E}_{j+1}(a_j,\omega),\ \partial_x\mathcal{E}_j(a_j,\omega) = \partial_x\mathcal{E}_{j+1}(a_j,\omega). \tag{29}$$

The electromagnetic fields are chosen as transverse-electric polarized fields [$E(x,t) = E_y(x,t)$]. For now, let us assume the general case of $N$ slabs, so that $j = 0, 1, \ldots, N, N+1$ with [$0 \equiv$ in] and [$N+1 \equiv$ out] as the background indices on the left and right side, respectively. The transmission problem is defined as

$$\begin{pmatrix} A_{in} \\ B_{in} \end{pmatrix} = \mathbf{M}_{in,out} \cdot \begin{pmatrix} A_{out} \\ B_{out} \end{pmatrix}, \tag{30}$$

with the *transfer matrix*

$$\mathbf{M}_{in,out} = \begin{pmatrix} m_{11}(\omega) & m_{12}(\omega) \\ m_{21}(\omega) & m_{22}(\omega) \end{pmatrix}, \tag{31}$$

which connects $A_{in}, B_{in}$ with $A_{out}, B_{out}$. In general, the corresponding transmission and reflection functions are

$$t(\omega) = \frac{A_{out}}{A_{in}} = \frac{1}{m_{11}(\omega)},\ r(\omega) = \frac{B_{in}}{A_{in}} = \frac{m_{21}(\omega)}{m_{11}(\omega)}. \tag{32}$$

In the case of outgoing boundary conditions, $A_{in} = B_{out} = 0$, which implies the condition

$$m_{11}(\omega) = 0, \tag{33}$$

whose complex solutions $\tilde{\omega}_\mu$ are the QNM frequencies of the problem. Moreover, these eigenfrequencies are exactly the complex poles of the transmission and reflection functions. An explicit expression for the matrix $\mathbf{M}_{in,out}$ can be obtained by subsequent multiplication of the transfer matrices from $j$ to $j+1$. For the special case of two dielectric barriers (which corresponds to three slabs), we obtain the determining equation:

$$\begin{aligned} 0 = {} & \beta_{1,+}^2\beta_{2,+}^2 - \beta_{1,-}^2\beta_{2,+}^2 e^{2ik_{R,1}L} \\ & + \beta_{1,-}^2\beta_{2,-}^2 e^{2ik_{R,1}L}e^{2ik_{R,2}L_p} - \beta_{1,+}^2\beta_{2,-}^2 e^{2ik_{R,2}L_p} \\ & + \beta_{1,+}\beta_{1,-}\beta_{2,+}\beta_{2,-}e^{2ik_B d}\left[e^{2ik_{R,1}L} - 1 + e^{2ik_{R,2}L_p}\right] \\ & - \beta_{1,+}\beta_{1,-}\beta_{2,+}\beta_{2,-}e^{2ik_B d}e^{2ik_{R,1}L}e^{2ik_{R,2}L_p}, \end{aligned} \tag{34}$$

where $\beta_{1,\pm} = n_{R,1} \pm n_B$, $\beta_{2,\pm} = n_{R,2} \pm n_B$, and $n_{R,1(2)}$ are the refractive indices of the first (second) barrier. Although this equation can only be solved analytically for certain conditions, it can be solved numerically in an exact manner. To do so, we will use the MPMATH package in Python [46], specifically the Muller algorithm from "mpmath.findroot."

#### 2. Modification to the single-barrier quasinormal mode frequencies

For a small height of the second barrier ($\delta \ll 1$), we can apply the first-order perturbation correction to obtain the QNM eigenfrequency change:

$$\tilde{k}_\mu^{(1)} = -\frac{\tilde{k}_\mu^{(0)}}{2}V\frac{\left[\tilde{f}_\mu^{(0)}(0)\right]^2}{2i\tilde{k}_\mu^{(0)}}e^{2i\tilde{k}_\mu^{(0)}d}\left[e^{2i\tilde{k}_\mu^{(0)}L_p} - 1\right]. \tag{35}$$

In contrast, the perturbation approach using regularization is

$$\tilde{k}_\mu^{(1)} = -\frac{\tilde{k}_\mu^{(0)}}{2}V\frac{\left[\tilde{f}_\mu^{(0)}(0)\right]^2}{2ik_\mu^{(0)}}e^{2ik_\mu^{(0)}d}\left[e^{2ik_\mu^{(0)}L_p} - 1\right], \tag{36}$$

where we have used $\tilde{F}_\mu'^{(0)}(x,\omega_\mu)$ instead of $\tilde{f}_\mu^{(0)}(x)$ for the evaluation of the overlap integral inside the perturbation region. It should be noted again that we cannot strictly use the total frequency-dependent regularized QNM $\tilde{F}_\mu^{(0)}(x,\omega)$ since a $\omega$-dependent QNM frequency change would be not meaningful, and we instead impose a pole approximation around the real part $\omega_\mu$. As was shown in Ref. [33]. for a single resonator as well as for a hybrid cavity system, this approximation is an excellent approximation to capture effects for frequencies in a regime of $\sim\pm 10\gamma_\mu^{(0)}$, around the center frequency $\omega_\mu^{(0)}$.

In the following, we will compare this mode correction (resulting in the modified eigenfrequency $\tilde{k}_\mu \approx \tilde{k}_\mu^{(0)} + \delta\tilde{k}_\mu^{(1)}$) to the full numerical solution obtained from Eq. (34).

We first consider the real part of the frequency change as function of distance $d$, with results shown in Fig. 6. Again, we choose an intermediate quality factor $Q \approx 20$ for the single-barrier cavity by setting $n_R = 2\pi$. The height of the second barrier is $\delta V$ with $\delta = 0.01$, so that one can safely assume validity of the perturbation approach. We recognize that the

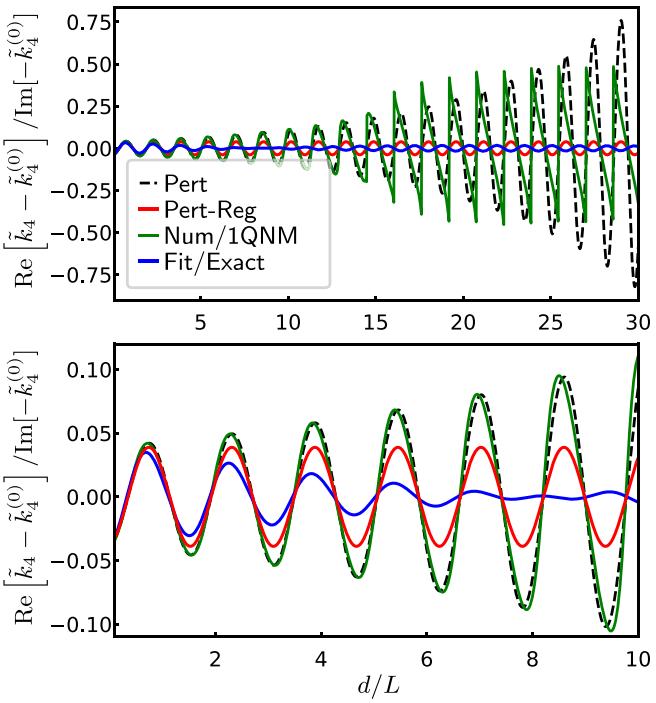


FIG. 6. Top: Real part of (normalized) eigenfrequency difference between the solution of the double-barrier structure ($\tilde{k}_\mu$) and the single-barrier structure ($\tilde{k}_\mu^{(0)}$) of the respective QNM with $\mu = 4$ as function of distance $d$ between the two barriers, using the numerical QNM solution, i.e., the numerically obtained eigenvalues of Eq. (34) (solid green curve, see legend), the complex QNM first-order perturbation result [black dashed curve, Eq. (35)], the results from the Lorentzian fit of $t(\omega)$ [solid blue curve, Eq. (32)], and the regularized QNM first-order perturbation result [solid red curve, Eq. (36)]. The first (second) barrier has a length $L$ ($L_\mathrm{p} = 0.1L$) and permittivity difference $\Delta\epsilon_\mathrm{c} = V$ ($\Delta\epsilon_\mathrm{p} = \delta V$ with $\delta = 0.01$) with $V = 4\pi^2 - 1$. Bottom: Enlargement (zoom in) of the top panel for smaller distances $d$.

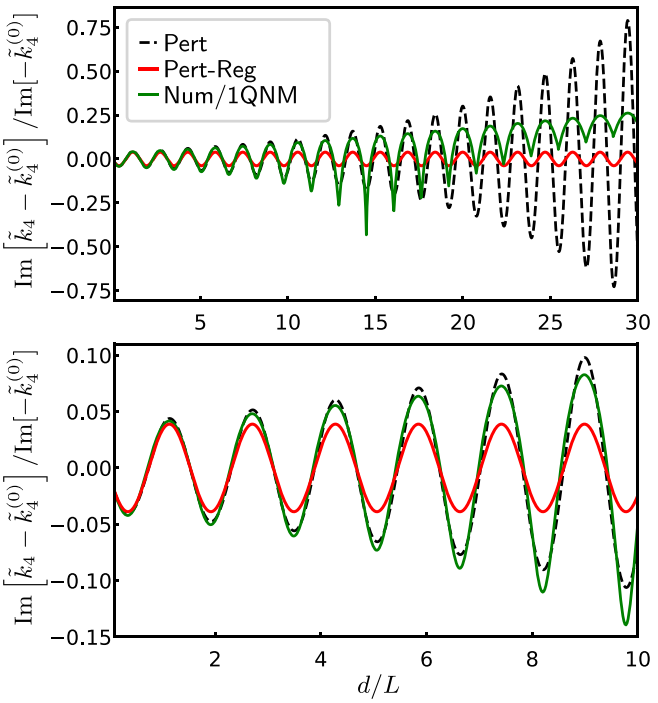


FIG. 7. Top: Imaginary part of (normalized) eigenfrequency difference between the solution of the double-barrier structure ($\tilde{k}_\mu$) and the single-barrier structure ($\tilde{k}_\mu^{(0)}$) of the respective QNM with $\mu = 4$ as function of distance $d$ between the two barriers, with the same setup as in Fig. 6, using the numerical QNM solution, i.e., the numerically obtained eigenvalues of Eq. (34) (solid green curve, see legend), the complex QNM perturbation result [black dashed curve, Eq. (35)], and the regularized QNM perturbation result [solid red curve, Eq. (36)]. Bottom: Enlargement of top panel for smaller distances $d$.

mode changes predicted by the full numerical pole solution are not exponentially growing, as expected. Simultaneously, perturbation theory using the naive expression involving the complex QNM $\tilde{f}_\mu$ fails to predict the correct frequency change for larger distances since $e^{2ik_\mu^{(0)}d}$ from Eq. (36) would be replaced by $e^{2i\tilde{k}_\mu^{(0)}d}$, leading to an exponential growth. However, when inspecting an enlargement around smaller distances [Fig. 6(b)], one can appreciate that the complex QNM approach agrees well with the full numerical approach. While the regularized QNM approach leads to a convergent result of the frequency change, it does not fully recover the results from the exact numerical approach. However, it recovers certain features of the multimode behavior, as will be discussed in Sec. V B 3. Indeed, we can see that the exact single QNM also fails to describe the full solution in this regime.

Next, we inspect the imaginary part of the frequency change, depicted in Fig. 7, which is related to mode dissipation. Similarly to the real part of the frequency change, the complex QNM perturbation result leads to an unphysical exponential growth of $\mathrm{Im}[\tilde{k}_\mu^{(1)}]$. The full numerical pole solution follows an exponential growing behavior for small distances, but it completely changes its form for $d/L > 10$. While the phase relation is identical to the perturbation results, the oscillations are clearly much more complex than simple cosine and sine functions. Furthermore, the average value is detuned from 0 to a positive value. This indicates further that the distance from the single barrier also changes the perturbation regime. This result is surprising and counterintuitive since one would expect a decreasing interaction between the two barriers for larger separations. However, there are some possible explanations for this behavior: (1) we observe that the numerical calculations become more unstable when increasing the distance between the two barriers since the initial value (single-barrier cavity) is expected to deviate exponentially for the complex QNM; (2) the concept of a single-mode picture becomes more and more vague because the increasing overlap from other modes can cause a general change in the frequency structure; (3) we are leaving the perturbation regime in the view of exponentially rising mode amplitudes (which is connected to the concept of complex modes).

#### *3. Multimode effects from the full transmission coefficient*

After comparing the solutions from the first-order perturbation correction to the full numerical pole solution, here we present a third method to obtain the frequency change by applying a Lorentzian fit to the transmission coefficient $t(\omega)$

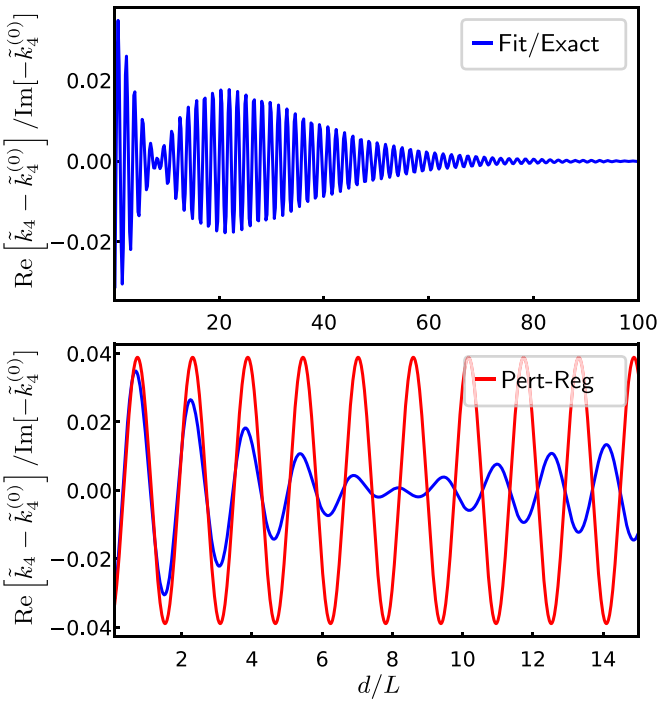


FIG. 8. Real part of the eigenfrequency difference between the single-barrier cavity and the double-barrier cavity (with unperturbed frequency $\tilde{k}_4^{(0)} = k_4^{(0)} - i\gamma_4^{(0)}/c$) with the same setup as in Fig. 6 using the regularized QNM perturbation result [bottom red curve, see legend, Eq. (36)], and a fit result to the exact transmission coefficient [blue curve, Eq. (32)] as function of distance $d$.

[cf. Eq. (32)] around the resonance of interest (without any mode approximations). This will not only capture the changes to the individual eigenfrequencies, but also the collective effects induced by other modes. These become especially significant for lower-$Q$ resonators. Note that coupled-mode effects were also investigated on the basis of the transfer matrix approach in more general structures with more than two barriers, allowing for complex interactions between the modes, e.g., in Ref. [47].

In Fig. 6, we have shown the corresponding results of the Lorentzian fit, which significantly differ from the predictions of the other methods. In Fig. 8, we show a more detailed analysis of the Lorentzian fit, and compare it to our proposed regularization of the QNM perturbation theory. We concentrate on the real part of the QNM eigenfrequency, i.e., the corresponding peak of the transmission coefficient around $\omega_4^{(0)}$. This is the more sensible quantity compared to the width. There are several features, that are captured by the fit results, which we summarize below:

(1) A first minimum appears for the frequency change, at $d/L \sim 8$, in the fit of the exact result. Note that we have also observed the same feature for several parameters of the perturbation, including a change in $\delta$ and $L_\mathrm{p}$ (as long as $\delta < 1$). Moreover, the particular position of the minimum is nearly independent of these parameters, while it is very sensitive to a change of the parameters of the single-barrier cavity, such as $n_\mathrm{R}$.

(2) We observe a phase shift for $d/L > 8$, after passing the *first minimum* location. To be precise, there is a phase difference of exactly $\Delta\phi = \pi/2$ compared to the QNM results (not only the regularized QNM approach).

(3) Aside from an additional oscillation, there is an overall damping of the eigenfrequency change, which likely reflects a multimode effect (fully captured by the transfer matrix results), where the changes from a single-mode picture are compensated.

A possible reason why the complex phase oscillations are not captured by the regularization of QNMs is because one has to impose a pole approximation to $\tilde{F}(x, \omega)$; this will likely remove some interference effects, which originate from other modal contributions in the exact transmission coefficient $t(\omega)$. In fact, this is not a failure of the regularization procedure itself since its impact was recently underlined in a second quantized QNM theory, in particular for the problem of deriving a proper input-output theory for three-dimensional and absorptive cavities. However, in that case, the fast oscillating terms (namely, $\exp[in_\mathrm{B}\omega(x-b)/c]$ for the one-dimensional analog and $x > b$) were taken into account without any pole approximation, resulting in a time retardation. In contrast, in the noted formalism of time-independent perturbation theory, it is simply impossible to recast these $\omega$-dependent terms into a temporal shift, and thus a pole approximation is applied to the total regularized QNM function. On the other hand, we emphasize again that from a discrete mode theory point of view, a mode quantity that depends on the continuous variable $\omega$ is not a meaningful quantity, and one is ultimately after a convergent few mode theory. Consequently, one has to make some approximations, depending upon the application and problem at hand.

### C. Three-dimensional metallic resonator

Next, we investigate a three-dimensional metallic dimer resonator, as depicted in Fig. 9(a), where we move a small spherical object with radius $r_\mathrm{p} = 30$ nm and permittivity difference $\Delta\epsilon_\mathrm{p} = 499$ ($n_\mathrm{B} = 1$) from a near-field region of the plasmonic dimer to the far-field region along the $x$ direction. Note that, more rigorously, one should also account for the nonlocal field corrections that are enforced by the continuity conditions of the electromagnetic field at the perturbation's boundary. For a (small) spherical shape, one can take into account the nonlocal effects by replacing $\Delta\epsilon_\mathrm{p}$ by an effective permittivity change [48,49], i.e., $\Delta\epsilon_\mathrm{p} \to 3\Delta\epsilon_\mathrm{p}\epsilon_\mathrm{B}/(3\epsilon_\mathrm{B} + \Delta\epsilon_\mathrm{p}) \equiv \Delta\epsilon_\mathrm{p}'$. In the presented example case, we derive $\Delta\epsilon_\mathrm{p}' \approx 2.98$.

To model the permittivity of the plasmonic dimer, we use the Drude model

$$\epsilon(\omega) = 1 - \frac{\omega_\mathrm{p}^2}{\omega(\omega + i\gamma_\mathrm{p})}, \tag{37}$$

with parameters that are somewhat similar to gold, with a plasma frequency $\omega_\mathrm{p} = \omega_\mathrm{p,Au} = 1.26 \times 10^{16}$ (rad/s) and $\gamma_\mathrm{p} = 3\gamma_\mathrm{p,Au} = 4.23 \times 10^{14}$ (rad/s). An efficient dipole-scattering approach is used to get the unperturbed QNM [50], which is performed with COMSOL [51]. The dominant mode of the plasmonic dimer in the optical spectral range of interest has a quality factor $Q^{(0)} \approx 7$, computed from $\hbar\tilde{\omega}^{(0)} = \hbar\omega^{(0)} - i\hbar\gamma^{(0)} = (2.0661 - 0.1477i)$ eV. From the results shown in Figs. 9(b) and 9(c), we can see a clear failure of simply using

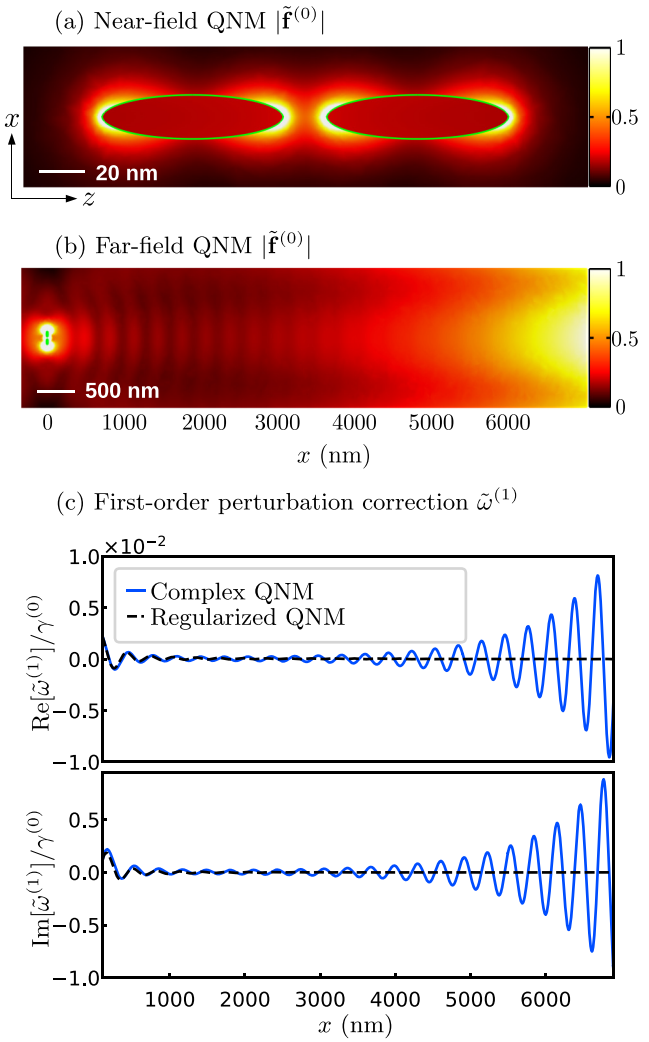


FIG. 9. (a) Near-field QNM (arb. units) $|\tilde{\mathbf{f}}^{(0)}|$ for a gold ellipsoid dimer with gap distance of 20 nm, as visualized schematically in Fig. 1. The center width and length of the ellipsoid are 20 and 80 nm, respectively. Note that the $z$ component is the dominant field component here, though all three components are included in $|\tilde{\mathbf{f}}^{(0)}|$. (b) Far-field QNM $|\tilde{\mathbf{f}}^{(0)}|$ of the same dimer (also in arb. units). The spatially diverging behavior is clearly shown in the far-field region, starting from around 3000 nm ($\sim 5\lambda^{(0)}$ of the current low-$Q$ example) away. (c) Real and imaginary parts of the first-order perturbation correction $\tilde{\omega}^{(1)}$ from $\tilde{k}^{(1)}$ [first line of Eq. (14)]. The perturbation region is a sphere with radius of 30 nm and the dielectric constant is $\epsilon_\mathrm{p} = 500$ ($\Delta\epsilon_\mathrm{p} = \epsilon_\mathrm{p} - \epsilon_\mathrm{B}$). Taking local field effect into account, we use $\Delta\epsilon_\mathrm{p} \to 3\Delta\epsilon_\mathrm{p}\epsilon_\mathrm{B}/(3\epsilon_\mathrm{B} + \Delta\epsilon_\mathrm{p}) \equiv \Delta\epsilon'_\mathrm{p} \approx 2.98$. The unperturbed resonance frequency of the dimer is given the values, e.g., $\hbar\tilde{\omega}^{(0)} = \hbar\omega^{(0)} - i\hbar\gamma^{(0)} = (2.0661 - 0.1477i)$ eV. The black dashed line reflects the result of the regularization, which is obtained by replacing $\tilde{\mathbf{f}}^{(0)}_\mu$ with $\tilde{\mathbf{F}}^{(0)}_\mu$ in Eq. (14) (see text).

$\tilde{\mathbf{f}}^{(0)} \equiv \tilde{\mathbf{f}}^{(0)}_\mu$, where the far-field QNM $|\tilde{\mathbf{f}}^{(0)}|$, as well as the real and imaginary parts of the first-order perturbation correction $\tilde{\omega}^{(1)} = c\tilde{k}^{(1)}$ [first line of Eq. (14)] are diverging.

In contrast to the QNM results, in Figs. 9(b) and 9(c), we obtain the correct far-field behavior when we use the regularized QNM fields. To obtain these regularized fields $\tilde{\mathbf{F}}^{(0)}_\mu$, we have employed an inverse Green function technique with a dipole source in real frequency space [29], where two different real frequencies are chosen as $\omega_{1/2} = \omega^{(0)} \pm 0.25\gamma^{(0)}$. We also note that, when using the regularized QNM approach, the results are convergent for larger distances ($x$) from the scattering object, although, for small distances both approaches result in equal changes in frequency induced by the perturbation. This confirms the behavior observed for the one-dimensional examples.

We remark that for the investigated structure (metal dimer plus a small spherical object in the far field), the results obtained from Eq. (14) (dipole approximation for the field inside the small perturbation region) are in very good agreement with the general formula Eq. (13).

## VI. DISCUSSION

The QNMs are defined as eigenfunctions of the open boundary problem, which form a complete set within the cavity region. The information of the "outside" is implicitly included in the open boundary conditions. The clear advantage over the so-called *modes of the universe* (and using continuous normal modes) is that, while the modes of the universe form a continuous set of modes, the QNMs form a *discrete* set. The disadvantage, however, is the spatial divergence of these mode eigenfunctions.

To elaborate further, in the usual treatment of open resonators, particularly in the field of open quantum systems, one makes an ansatz: $H = H_0 + \lambda H_I$, where $H_I$ is the coupling element with strength $\lambda$, and $H_0$ contains the energies of the isolated closed system and bath. In a second-order Born-Markov treatment of the interaction, one arrives at an effective description of the system, where the small perturbation turns into a decay rate of the system, which could in turn be regarded as the QNM imaginary part of the eigenfrequency. However, in contrast to this description, the QNMs are not restricted to small imaginary parts, and the inherent mode dissipation leads to much richer properties of the QNMs (such as an unconjugated form for the normalization), which is not covered at all by the phenomenological system-bath ansatz [43]. The unconjugated QNM expansion retains essential phase information, which can give rise to few mode Fano-type resonances [52–54] and unusual power flow from a point dipole and quantum emitter [55].

On the other hand, regularization of the open-cavity modes brings back in the properties of the background through the continuous real-valued frequency $\omega$. From a different viewpoint, the QNMs' basis is extended by a plane-wave expansion of the background Green function $\mathbf{G}_\mathrm{B}$, and again becomes continuous. Thus, in order to fully describe processes that are directly related to the "background," e.g., measurements at detectors well outside of the cavity region, it seems to be inevitable to use an expansion in terms of propagation waves in real frequency space, even though the whole open boundary problem is solved with QNMs on their own. From a more practical perspective, one is often interested in complicated background and cavity structures, such as a waveguide-cavity system within a photonic crystal structure. In such cases, the regularized QNMs would not be formed by simple plane waves, but by waveguide Bloch modes, reflecting the periodic structure of the photonic crystal as well as the

waveguide properties [56]. Those cases are naturally included by the proposed regularization approaches since there appears no restriction to the background Green function, as long as there exists an analytical form, e.g., the waveguide Green function in terms of Bloch modes.

The problem of requiring additional degrees need not only be formulated in terms of the Green function, but also in terms of the electric field. Indeed, if we inspect the surface integral representation of the regularization [Eq. (20)] in the time domain, we can formulate the total electric field as

$$E(x>b,t) = 2\pi i \sum_\mu a_\mu(t=0)\tilde{f}_\mu(b) \times \int_{-\infty}^{\infty} d\omega \frac{e^{-i\omega(t-n_\mathrm{B}[x-b]/c)}}{\tilde{\omega}_\mu - \omega}. \tag{38}$$

For $t>0$, we can apply the residue theorem to obtain

$$E(x>b,t) = \sum_\mu a_\mu(t)\tilde{f}_\mu(b)e^{in_\mathrm{B}\tilde{\omega}_\mu(x-b)/c} = \sum_\mu a_\mu(t)\tilde{f}_\mu(x), \tag{39}$$

for $t > n_\mathrm{B}[x-b]/c$ and zero otherwise. Thus, this gives another hint that the QNMs outside the resonator cannot be formulated in terms of the system QNMs alone (i.e., the QNMs inside the resonator), but they need additional degrees of freedom. Note there is a clear difference when using the regularization compared to simply assuming completeness of the QNMs over all space, i.e., assuming Eq. (39) for all $t>0$ and $x$.

The divergent behavior of the eigenfrequency change is obviously also induced by the presence of the unconjugated form of the QNM expansion, where $\tilde{f}_\mu\tilde{f}_\mu$ instead of $|\tilde{f}_\mu|^2$ appears in the first-order correction terms [cf. Eq. (13)]. An interesting alternative Green function expansion, by means of a conjugated form, can be formulated based on a fundamental Green function relation (cf. Appendix B) through

$$\mathrm{Im}[G(x,y,\omega)] = n_\mathrm{B}\frac{c}{\omega}[G(x,a,\omega)G^*(a,y,\omega) + G(x,b,\omega)G^*(b,y,\omega)] \tag{40}$$

for $a<x,y<b$, which was recognized in Ref. [57] for the one-dimensional case with nondispersive media. Nearly two decades later, an analogous relation for three-dimensional absorptive and leaky structures was found to be a necessary representation for QNM quantization, in which a well-defined QNM Fock space can be defined [31,32,58].

Using this knowledge from previous works, one can then utilize the Kramers-Kronig relations

$$\mathrm{Re}[G(x,x_0,\omega)] = \frac{1}{\pi}\mathrm{P}\int_{-\infty}^{\infty} d\omega' \frac{\mathrm{Im}[G(x,x_0,\omega')]}{\omega'-\omega}, \tag{41}$$

where P is the Cauchy principal value of the integral, to obtain the corresponding real part of the Green function by means of complex contour integration techniques. This would lead to the representation (cf. Appendix C)

$$G(x,x_0,\omega) = \sum_{\mu\eta}\tilde{f}_\mu(x)K_{\mu\eta}(\omega)\tilde{f}^*_\eta(x_0), \tag{42}$$

where

$$K_{\mu\eta}(\omega) = \frac{in_\mathrm{B}c\tilde{\omega}_\mu}{2}\frac{\tilde{f}_\mu(a)\tilde{f}^*_\eta(a)+\tilde{f}_\mu(b)\tilde{f}^*_\eta(b)}{(\tilde{\omega}_\mu-\tilde{\omega}^*_\eta)(\omega-\tilde{\omega}_\mu)}. \tag{43}$$

We see a clear difference over the unconjugated form, in that a double sum over all QNMs appears. The dissipative character is now expressed in terms of off-diagonal terms, that depend on QNM functions on the cavity boundary. Indeed, in the NM limit [$\gamma_\mu \to 0$ and $\tilde{f}_\mu(a), \tilde{f}_\mu(b) \to 0$], the off-diagonal elements of $K_{\mu\eta}(\omega)$ tend to zero, and we are left with the diagonal elements

$$K_\mu(\omega) = \frac{n_\mathrm{B}c\tilde{\omega}_\mu}{2}\frac{\tilde{f}_\mu(a)\tilde{f}^*_\mu(a)+\tilde{f}_\mu(b)\tilde{f}^*_\mu(b)}{2\gamma_\mu(\tilde{\omega}_\mu-\omega)}. \tag{44}$$

In the lossless limit, we can precisely derive [57]

$$n_\mathrm{B}c\frac{|\tilde{f}_\mu(a)|^2+|\tilde{f}_\mu(b)|^2}{2\gamma_\mu} \to 1, \tag{45}$$

for all $\mu$, so that

$$K_{\mu\eta}(\omega) \to \frac{\omega_\mu}{2(\omega_\mu-\omega)}\delta_{\mu\eta} \tag{46}$$

and

$$G(x,x_0,\omega) \to \sum_\mu \frac{\omega_\mu f_\mu(x)f^*_\mu(x_0)}{2(\omega_\mu-\omega)}. \tag{47}$$

If we now split the sum into $\mu=0$, $\mu>0$, and $\mu<0$, we obtain

$$G(x,x_0,\omega) \to \sum_{\mu>0} \frac{\omega^2_\mu f_\mu(x)f^*_\mu(x_0)}{\omega^2_\mu-\omega^2}, \tag{48}$$

which is indeed identical to the NM expansion of the Green function. Note, here we have assumed that the NM functions have a position-independent trivial phase, so that $f_\mu(x)f^*_\mu(x_0) = f^*_\mu(x)f_\mu(x_0)$, and have used $\omega_0 \to 0$.

Note that such a nondiagonal form of the Green function can also be derived for the more general case of three-dimensional and absorptive geometries, as shown in Appendix D. Although the conjugated form seems to remove a potential divergent behavior, one must note that (i) the approximation to a few QNM expansion is not equally valid in both representations, and (ii) the nondiagonal form prevents one from adapting to the perturbation theory presented in Ref. [43].

## VII. CONCLUSIONS

We have discussed and presented different potential solutions to the problem of perturbation theory for open resonators, using QNMs, when perturbations are added outside the resonator (and potentially far outside the resonator). We showed results for the (complex) frequency change of the QNM by including a perturbation outside of the resonator region, for (i) a one-dimensional double-barrier system, and (ii) a three-dimensional plasmonic dimer structure. The first example serves as our main example system since it allows important analytical insight into the underlying physics of the QNMs and the solutions in terms of the scattered fields.

It was demonstrated that naively adopting the system QNM expansion of the Green function for positions outside the resonator yields an unphysical exponential growth of the QNM eigenfrequency change. This is induced by the dissipative nature of QNMs. We also showed how a regularization of QNMs, in terms of a function of a continuous variable for each QNM, can remove such a divergent behavior of the QNMs. While neither the few QNMs or few regularized QNMs constitute an exact solution, or can exactly mimic the behavior that is observed using the fit to the full solution (cf. Fig. 8), we have shown how one can benefit from using both of these representations. In fact, the applicability of the few regularized QNM theory has a clear advantage over the fit of the full transmission coefficient. This is because it is independent of the incident field, and lends itself to solving both classical and quantum optical problems, the latter of which requires the use of quantized modes [31]. Such a combination of complex QNMs and a regularization procedure is particularly important for more complicated structures, such as coupled cavity-waveguide structures and a further theory development building upon previous works on coupled QNM frameworks [27,59] will be an important task for future investigations.

The perturbation picture can also be understood, in the quantum picture, as the problem of having a quantum dipole emitter moved away from the cavity, where one needs (*requires*) the regularized QNMs. To elaborate, in these applications one usually investigates the change of the emitter's linewidth and frequency through a (perturbative) second-order Born-Markov approach (weak coupling) [31,60,61]. However, in our current investigations shown here, we looked at this from a different perspective, namely, how the cavity frequency and linewidth change in the presence of the emitter (perturbation) or, more generally, a perturbation object. Certainly, one would expect the same kind of fix that we adopt for the perturbed modes, i.e., a regularized cavity mode that is inherently dissipative. Since the emitter has a finite linewidth, its respective radiation will also diverge in space. In a quantum perspective, there might be a deeper connection between a quantization of dissipative QNMs and a collection of emitters [62,63], where the rigorous treatment of loss leads to an inherent coupling. In the former approach, the regularization of QNMs (in the form that is presented here) is a crucial part of the respective quantization procedure.

## ACKNOWLEDGMENTS

We acknowledge funding from Queen's University, Canada, the Canadian Foundation for Innovation (CFI), the Natural Sciences and Engineering Research Council of Canada (NSERC), and CMC Microsystems for the provision of COMSOL Multiphysics. We also acknowledge support from the Alexander von Humboldt Foundation through a Humboldt Research Award.

## APPENDIX A: DERIVATION OF THE SURFACE REPRESENTATION OF THE REGULARIZED QNM FIELD

In this Appendix, we prove the equivalence of Eqs. (7) and (11). We start with the general solution of $\boldsymbol{\mathcal{E}}(\mathbf{R},\omega)$ from the scattering problem,

$$\boldsymbol{\mathcal{E}}(\mathbf{R},\omega)=\int_{\mathcal{V}'}d^3r\,\Delta\epsilon(\mathbf{r},\omega)\mathbf{G}_{\mathrm{B}}(\mathbf{R},\mathbf{r},\omega)\cdot\boldsymbol{\mathcal{E}}(\mathbf{r},\omega),\tag{A1}$$

where we have chosen $\mathcal{V}'$ as a volume that is supported by $\Delta\epsilon$, i.e., where $\Delta\epsilon(\mathbf{r})\neq 0$. Next, we rewrite the above equation as

$$\begin{aligned}\boldsymbol{\mathcal{E}}(\mathbf{R},\omega)=&\int_{\mathcal{V}'}d^3r\,\epsilon(\mathbf{r},\omega)\mathbf{G}_{\mathrm{B}}(\mathbf{R},\mathbf{r},\omega)\cdot\boldsymbol{\mathcal{E}}(\mathbf{r},\omega)\\&-\int_{\mathcal{V}'}d^3r\,\epsilon_{\mathrm{B}}\mathbf{G}_{\mathrm{B}}(\mathbf{R},\mathbf{r},\omega)\cdot\boldsymbol{\mathcal{E}}(\mathbf{r},\omega).\end{aligned}\tag{A2}$$

Using the Helmholtz equation with $\boldsymbol{\mathcal{E}}(\mathbf{r},\omega)$ and $\mathbf{G}_{\mathrm{B}}(\mathbf{R},\mathbf{r},\omega)$, this leads to

$$\begin{aligned}\boldsymbol{\mathcal{E}}(\mathbf{R},\omega)=&\frac{c^2}{\omega^2}\int_{\mathcal{V}'}d^3r\,\mathbf{G}_{\mathrm{B}}(\mathbf{R},\mathbf{r},\omega)\cdot[\boldsymbol{\nabla}\times\boldsymbol{\nabla}\times\boldsymbol{\mathcal{E}}(\mathbf{r},\omega)]\\&-\frac{c^2}{\omega^2}\int_{\mathcal{V}'}d^3r[\boldsymbol{\nabla}\times\boldsymbol{\nabla}\times\mathbf{G}_{\mathrm{B}}(\mathbf{r},\mathbf{R},\omega)]^{\mathrm{t}}\cdot\boldsymbol{\mathcal{E}}(\mathbf{r},\omega)\\&+\int_{\mathcal{V}'}d^3r\,\delta(\mathbf{r}-\mathbf{R})\boldsymbol{\mathcal{E}}(\mathbf{r},\omega).\end{aligned}\tag{A3}$$

The last term vanishes when we choose $\mathbf{R}$, such that $\mathbf{R}\neq\mathcal{V}'$. Finally, we utilize the second dyadic-vector Green's theorem to reduce the volume integral to a surface integral over $\mathcal{S}'$:

$$\begin{aligned}\boldsymbol{\mathcal{E}}(\mathbf{R},\omega)=&\frac{c^2}{\omega^2}\int_{\mathcal{S}'}dA_{\mathbf{s}}\mathbf{G}_{\mathrm{B}}(\mathbf{R},\mathbf{s},\omega)]\cdot[\mathbf{n}\times\boldsymbol{\nabla}\times\boldsymbol{\mathcal{E}}(\mathbf{s},\omega)]\\&-\frac{c^2}{\omega^2}\int_{\mathcal{S}'}dA_{\mathbf{s}}[\mathbf{n}\times\boldsymbol{\nabla}\times\mathbf{G}_{\mathrm{B}}(\mathbf{r},\mathbf{R},\omega)]^{\mathrm{t}}\cdot\boldsymbol{\mathcal{E}}(\mathbf{s},\omega).\end{aligned}\tag{A4}$$

The important point here is that the appearing functions and their derivatives need to be continuous in $\mathcal{V}'$, which prevents one from extending the volume $\mathcal{V}'$, in which $\Delta\epsilon$ becomes discontinuous.

If we now assume completeness of QNMs at $\mathcal{S}'$, we can reformulate the above expression as $\boldsymbol{\mathcal{E}}(\mathbf{R},\omega)=\sum_\mu a_\mu^{(0)}(\omega)\tilde{\mathbf{F}}_\mu'^{(0)}(\mathbf{r},\omega)$, where $\tilde{\mathbf{F}}_\mu'^{(0)}(\mathbf{r},\omega)$ is precisely the regularized QNM function from Eq. (12). We emphasize that the same derivation holds true on the level of the Green function, where the starting point would be

$$\begin{aligned}\mathbf{G}^{\perp}(\mathbf{R},\mathbf{r})=&\mathbf{G}_{\mathrm{B}}^{\perp}(\mathbf{R},\mathbf{r})\\&+\int d^3s\,\Delta\epsilon(\mathbf{s})\mathbf{G}_{\mathrm{B}}(\mathbf{R},\mathbf{s})\cdot\mathbf{G}^{\perp}(\mathbf{s},\mathbf{r}),\end{aligned}\tag{A5}$$

with an implicit dependence on $\omega$.

## APPENDIX B: PROOF OF GREEN'S IDENTITIES

Here we will prove the Green's identity from Eq. (40). In one spatial dimension, the Helmholtz equation of the Green function reduces to

$$\partial_x^2G(x,x')+\frac{\omega^2}{c^2}\epsilon(x)G(x,x')=-\frac{\omega^2}{c^2}\delta(x-x'),\tag{B1}$$

with an implicit $\omega$ dependence for the Green function and the permittivity. The associated conjugated form is

$$\partial_x^2 G^*(x,x'') + \frac{\omega^2}{c^2}\epsilon^*(x)G^*(x,x'') = -\frac{\omega^2}{c^2}\delta(x-x''). \quad \text{(B2)}$$

For now, we assume a real permittivity $\epsilon(x) \in \mathbb{R}$ without any absorption. Note that, in principle, this is an approximation and only valid in a limited frequency range. Multiplying the first equation with $G^*(x,x'')$ and the second equation with $G(x,x')$, then subtracting both resulting equations and integrating over $[a,b]$, leads to

$$2i\frac{\omega^2}{c^2}\mathrm{Im}[G(x',x'')] = \int_a^b dx[\partial_x^2 G(x,x')]G^*(x,x'') - G(x,x')[\partial_x^2 G^*(x,x'')], \quad \text{(B3)}$$

where we have assumed $x', x'' \in [a,b]$. Utilizing partial integration techniques, we can reformulate Eq. (B3) as

$$2i\frac{\omega^2}{c^2}\mathrm{Im}[G(x',x'')] = [\partial_x G(x,x')]G^*(x,x'')|_a^b - G(x,x')[\partial_x G^*(x,x'')]|_a^b. \quad \text{(B4)}$$

Next, we use the outgoing boundary conditions to simplify this expression as

$$\mathrm{Im}[G(x',x'')] = n_\mathrm{B}\frac{c}{\omega}[G(b,x')G^*(b,x'') + G(a,x')G^*(a,x'')], \quad \text{(B5)}$$

which proves Eq. (40).

## APPENDIX C: COMPLEX CONTOUR INTEGRATION

In this Appendix, we derive the principal value integrals that appear in the Kramers-Kronig relations, Eq. (41), by using the nondiagonal form of the imaginary part of the Green function in one spatial dimension. The relevant frequency integral can be summarized as

$$T_{\mu\eta}(\omega) = \mathrm{P}\int_{-\infty}^{\infty} d\omega' \frac{\omega'}{(\omega'-\omega)(\omega'-\tilde{\omega}_\mu)(\omega'-\tilde{\omega}_\eta^*)}, \quad \text{(C1)}$$

which can be solved analytically via complex contour integration. Specifically, we choose a curve $C(\epsilon)$, describing a half-circle with radius $R > |\omega| + \epsilon$ in the upper half-plane with another smaller half-circle centered at $\omega$ with radius $\epsilon$ (cf. Fig. 10). The contour shall contain the eigenfrequency $\tilde{\omega}_\eta^*$.

Defining the integrand as $K(\omega)$, we write the complex contour integration:

$$\begin{aligned}\oint_{C(\epsilon)} dz\, K(z) &= \int_{-R}^{\omega-\epsilon} d\omega' K(\omega') + \int_{\omega+\epsilon}^{R} d\omega' K(\omega') \\ &+ iR^2\int_0^\pi d\theta \frac{e^{2i\theta}}{(Re^{i\theta}-\omega)(Re^{i\theta}-\tilde{\omega}_\mu)(Re^{i\theta}-\tilde{\omega}_\eta^*)} \\ &- i\epsilon\int_0^\pi d\phi \frac{e^{i\phi}(\omega+\epsilon e^{i\phi})}{\epsilon e^{i\phi}(\omega+\epsilon e^{i\phi}-\tilde{\omega}_\mu)(\omega+\epsilon e^{i\phi}-\tilde{\omega}_\eta^*)}.\end{aligned} \quad \text{(C2)}$$

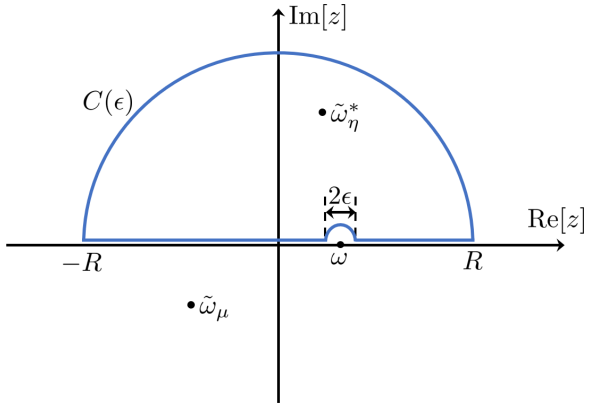


FIG. 10. Visualization of the contour integration in the complex plane for the one-dimensional and nonabsorptive cases. The contour $C(\epsilon)$ is enclosing the set of a half-circle in the upper half-plane with radius $R$ (and center point $z = 0$) subtracted by a smaller half-circle in the upper half-plane with radius $\epsilon$ (and center point $z = \omega$).

In the limit $R \to \infty$, the second contribution vanishes since it scales with $1/R$. In the limit $\epsilon \to 0$, the fourth contribution remains finite and gives

$$-i\pi\frac{\omega}{(\omega-\tilde{\omega}_\mu)(\omega-\tilde{\omega}_\eta^*)}. \quad \text{(C3)}$$

In the limit $R \to \infty$ and $\epsilon \to 0$, the sum of the first and second contributions exactly yields the principal value of the integral of interest. Using the residue theorem, we can calculate the contour integral as

$$\oint_{C(\epsilon)} dz\, K(z) = 2i\pi\frac{\tilde{\omega}_\eta^*}{\tilde{\omega}_\eta^*-\tilde{\omega}_\mu}\frac{1}{\tilde{\omega}_\eta^*-\omega}, \quad \text{(C4)}$$

so that

$$T_{\mu\eta}(\omega) = \frac{2i\pi\tilde{\omega}_\eta^*(\omega-\tilde{\omega}_\mu) + i\pi\omega(\tilde{\omega}_\mu-\tilde{\omega}_\eta^*)}{(\tilde{\omega}_\mu-\tilde{\omega}_\eta^*)(\omega-\tilde{\omega}_\eta^*)(\omega-\tilde{\omega}_\mu)}. \quad \text{(C5)}$$

Inserting back into the Kramers-Kronig relations and combining with the imaginary part of the Green function leads to Eq. (42).

## APPENDIX D: THREE-DIMENSIONAL AND ABSORPTIVE CASE

In this Appendix, we will present the derivation of the nondiagonal QNM Green function for the more general case of a three-dimensional and absorptive medium. This includes a generalization of the complex contour integration presented in Appendix C.

The fundamental Green function relation in one dimension [i.e., Eq. (42)] is generalized to

$$\begin{aligned}\mathrm{Im}[\mathbf{G}(\mathbf{r},\mathbf{r}')] &= \frac{c^2}{2i\omega^2}\int_{S(V)} dA_\mathbf{s}\{[\mathbf{n}_\mathbf{s}\times\mathbf{G}(\mathbf{s},\mathbf{r})]^\mathrm{t}\cdot[\boldsymbol{\nabla}_\mathbf{s}\times\mathbf{G}^*(\mathbf{s},\mathbf{r}')] \\ &- [\boldsymbol{\nabla}_\mathbf{s}\times\mathbf{G}(\mathbf{s},\mathbf{r})]^\mathrm{t}\cdot[\mathbf{n}_\mathbf{s}\times\mathbf{G}^*(\mathbf{s},\mathbf{r}')]\} \\ &+ \int_V d\mathbf{s}\,\epsilon_I(\mathbf{s})\mathbf{G}(\mathbf{r},\mathbf{s})\cdot\mathbf{G}^*(\mathbf{s},\mathbf{r}')\end{aligned} \quad \text{(D1)}$$

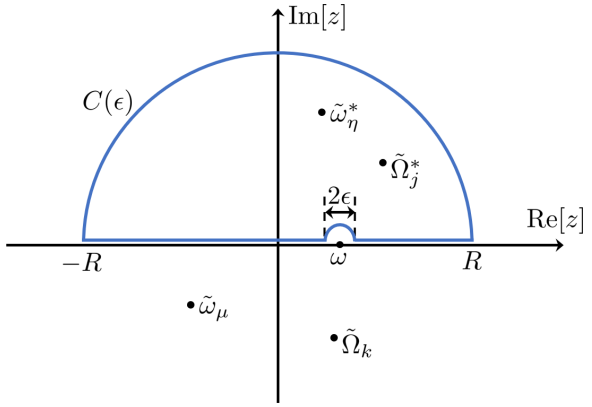


FIG. 11. Visualization of the contour integration in the complex plane for the three-dimensional and absorptive case. The contour $C(\epsilon)$ is enclosing the set of a half-circle in the upper half-plane with radius $R$ (and center point $z = 0$) subtracted by a smaller half-circle in the upper half-plane with radius $\epsilon$ (and center point $z = \omega$).

for $\mathbf{r}, \mathbf{r}_0 \in V$, which was more rigorously derived in Ref. [32], by introducing a sequence of permittivity functions.

Similarly to the one-dimensional case, one can utilize the Kramers-Kronig relations to obtain the corresponding real part of the Green function, $\mathrm{Re}[\mathbf{G}(\mathbf{r}, \mathbf{r}', \omega)]$, through

$$\mathrm{Re}[\mathbf{G}(\mathbf{r}, \mathbf{r}', \omega)] = \frac{1}{\pi} \mathrm{P} \int_{-\infty}^{\infty} d\omega' \frac{\mathrm{Im}[\mathbf{G}(\mathbf{r}, \mathbf{r}', \omega')]}{\omega' - \omega}, \tag{D2}$$

where, once again, P is the Cauchy principal value of the integral. Here, we should note that, in contrast to the more simpler nonabsorptive case, there is an additional $\omega$ kernel in the volume integral part, namely, the imaginary part of the permittivity $\epsilon_I(\mathbf{r}, \omega)$. Generally, $\epsilon(\mathbf{r}, \omega)$ is a causal function, i.e., an analytical function in the complex upper half-plane and has the form [64,65]

$$\epsilon(\mathbf{r}, \omega) = \epsilon_\infty(\mathbf{r}) + \sum_j \frac{\sigma_j(\mathbf{r})}{\omega - \tilde{\Omega}_j}, \tag{D3}$$

where $\tilde{\Omega}_j$ are the complex poles of the material of interest with negative imaginary part, and $\sigma_j(\mathbf{r})$ is a weighting function and $\epsilon_\infty(\mathbf{r}) = \epsilon(\mathbf{r}, \omega \to \infty)$ is the high-frequency limit.

Next, we first inspect the contribution associated with the surface integral term, where one has to solve the frequency integral

$$T^{\mathrm{sur}}_{\mu\eta}(\omega) = \mathrm{P} \int_{-\infty}^{\infty} d\omega' \frac{1}{(\omega' - \omega)(\omega' - \tilde{\omega}_\mu)(\omega' - \tilde{\omega}_\eta^*)}. \tag{D4}$$

This integral can be solved analytically via complex contour integration. Specifically, we choose a curve $C(\epsilon)$, describing a half-circle with radius $R > |\omega| + \epsilon$ in the upper half-plane with another smaller half-circle centered at $\omega$ with radius $\epsilon$ (cf. Fig. 11). The contour shall contain the eigenfrequency $\tilde{\omega}_\eta^*$.

Defining the integrand as $K^{\mathrm{sur}}(\omega)$, we manipulate the complex contour integration as

$$\begin{aligned} &\oint_{C(\epsilon)} dz\, K^{\mathrm{sur}}(z) \\ &= \int_{-R}^{\omega-\epsilon} d\omega' K^{\mathrm{sur}}(\omega') + \int_{\omega+\epsilon}^{R} d\omega' K^{\mathrm{sur}}(\omega') \\ &\quad + iR \int_0^\pi d\theta \frac{e^{i\theta}}{(Re^{i\theta} - \omega)(Re^{i\theta} - \tilde{\omega}_\mu)(Re^{i\theta} - \tilde{\omega}_\eta^*)} \\ &\quad - i\epsilon \int_0^\pi d\phi \frac{e^{i\phi}}{\epsilon e^{i\phi}(\omega + \epsilon e^{i\phi} - \tilde{\omega}_\mu)(\omega + \epsilon e^{i\phi} - \tilde{\omega}_\eta^*)}, \end{aligned} \tag{D5}$$

where we have parametrized the half-circles via $z = Re^{i\theta}$ and $z = \epsilon e^{i\phi}$, respectively. In the limit $R \to \infty$, the third contribution vanishes since it scales with $1/R^2$. In the limit $\epsilon \to 0$, the fourth contribution remains finite and gives

$$-i\pi \frac{1}{(\omega - \tilde{\omega}_\mu)(\omega - \tilde{\omega}_\eta^*)}. \tag{D6}$$

In the limit $R \to \infty$ and $\epsilon \to 0$, the first and second contributions yield exactly the principal value of the integral of interest. Using the residue theorem, we can calculate the contour integral as

$$\oint_{C(\epsilon)} dz\, K^{\mathrm{sur}}(z) = 2i\pi \frac{1}{(\tilde{\omega}_\eta^* - \tilde{\omega}_\mu)(\tilde{\omega}_\eta^* - \omega)}, \tag{D7}$$

so that

$$T^{\mathrm{sur}}_{\mu\eta}(\omega) = \frac{2i\pi(\omega - \tilde{\omega}_\mu) + i\pi(\tilde{\omega}_\mu - \tilde{\omega}_\eta^*)}{(\tilde{\omega}_\mu - \tilde{\omega}_\eta^*)(\omega - \tilde{\omega}_\eta^*)(\omega - \tilde{\omega}_\mu)}. \tag{D8}$$

Next, we turn to the volume integral contribution, where the appearing frequency integral is given by

$$T^{\mathrm{vol}}_{\mu\eta}(\omega) = \frac{1}{2i} \mathcal{P} \int_{-\infty}^{\infty} d\omega' \frac{[\omega']^2 [\epsilon(\mathbf{r}, \omega') - \epsilon^*(\mathbf{r}, \omega')]}{(\omega' - \omega)(\omega' - \tilde{\omega}_\mu)(\omega' - \tilde{\omega}_\eta^*)}, \tag{D9}$$

with an additional frequency-dependent permittivity function in the numerator. Using the fact that $\epsilon(\mathbf{r}, \omega')$ has the form in Eq. (D3), we derive

$$\begin{aligned} T^{\mathrm{vol}}_{\mu\eta}(\omega) = &\frac{2\pi\tilde{\omega}_\eta^{*2}\chi(\mathbf{r}, \tilde{\omega}_\eta^*)(\omega - \tilde{\omega}_\mu) + \pi\omega^2\chi(\mathbf{r}, \omega)(\tilde{\omega}_\mu - \tilde{\omega}_\eta^*)}{2(\tilde{\omega}_\mu - \tilde{\omega}_\eta^*)(\omega - \tilde{\omega}_\eta^*)(\omega - \tilde{\omega}_\mu)} \\ &- \sum_j T^{\mathrm{vol,j}}_{\mu\eta}(\omega), \end{aligned} \tag{D10}$$

where $\chi(\mathbf{r}, \omega) = \epsilon(\mathbf{r}, \omega) - \epsilon_\infty(\mathbf{r})$ is the susceptibility and

$$T^{\mathrm{vol,j}}_{\mu\eta}(\omega) = \frac{1}{2i} \mathrm{P} \int_{-\infty}^{\infty} d\omega' \frac{[\omega']^2 \chi_j^*(\mathbf{r}, \omega')}{(\omega' - \omega)(\omega' - \tilde{\omega}_\mu)(\omega' - \tilde{\omega}_\eta^*)}. \tag{D11}$$

Note that there is an additional pole $\tilde{\Omega}_j^*$ in the upper complex half-plane in this expression (as visualized in Fig. 11), so

that the residue theorem yields

$$\oint_{C(\epsilon)} dz\, K^{\mathrm{vol,j}}(z) = \pi \frac{[\tilde{\Omega}_j^*]^2 \sigma_j(\mathbf{r})}{(\tilde{\Omega}_j^* - \tilde{\omega}_\mu)(\tilde{\Omega}_j^* - \omega)(\tilde{\Omega}_j^* - \tilde{\omega}_\eta^*)} + \pi \frac{[\tilde{\omega}_\eta^*]^2 \chi_j^*(\mathbf{r}, \tilde{\omega}_\eta^*)}{(\tilde{\omega}_\eta^* - \tilde{\omega}_\mu)(\tilde{\omega}_\eta^* - \omega)}. \tag{D12}$$

Consequently, we obtain

$$T_{\mu\eta}^{\mathrm{vol,j}}(\omega) = \pi \frac{[\tilde{\Omega}_j^*]^2 \sigma_j(\mathbf{r})}{(\tilde{\Omega}_j^* - \tilde{\omega}_\mu)(\tilde{\Omega}_j^* - \omega)(\tilde{\Omega}_j^* - \tilde{\omega}_\eta^*)} + \pi \frac{[\tilde{\omega}_\eta^*]^2 \chi_j^*(\mathbf{r}, \tilde{\omega}_\eta^*)}{(\tilde{\omega}_\eta^* - \tilde{\omega}_\mu)(\tilde{\omega}_\eta^* - \omega)} + \frac{\pi}{2} \frac{\omega^2 \chi_j^*(\mathbf{r}, \omega)}{(\omega - \tilde{\omega}_\mu)(\omega - \tilde{\omega}_\eta^*)}. \tag{D13}$$

Summarizing all terms, we arrive at

$$T_{\mu\eta}^{\mathrm{vol}}(\omega) = \frac{2i\pi \tilde{\omega}_\eta^{*2} \epsilon_I(\mathbf{r}, \tilde{\omega}_\eta^*)(\omega - \tilde{\omega}_\mu) + i\pi\omega^2 \epsilon_I(\mathbf{r}, \omega)(\tilde{\omega}_\mu - \tilde{\omega}_\eta^*)}{(\tilde{\omega}_\mu - \tilde{\omega}_\eta^*)(\omega - \tilde{\omega}_\eta^*)(\omega - \tilde{\omega}_\mu)} + \pi \frac{[\tilde{\Omega}_j^*]^2 \sigma_j(\mathbf{r})}{(\tilde{\Omega}_j^* - \tilde{\omega}_\mu)(\tilde{\Omega}_j^* - \omega)(\tilde{\Omega}_j^* - \tilde{\omega}_\eta^*)}. \tag{D14}$$

Finally, inserting these back into the Kramers-Kronig relation (D2), we obtain

$$\mathbf{G}(\mathbf{r}, \mathbf{r}', \omega) = \sum_{\mu\eta} \tilde{\mathbf{f}}_\mu(\mathbf{r}) K_{\mu\eta}(\omega) \tilde{\mathbf{f}}_\eta^*(\mathbf{r}'), \tag{D15}$$

where $K_{\mu\eta}(\omega) = K_{\mu\eta}^{\mathrm{sur}}(\omega) + K_{\mu\eta}^{\mathrm{vol}}(\omega)$; the surface term is defined from

$$K_{\mu\eta}^{\mathrm{sur}}(\omega) = \frac{c^2 \int_{\mathcal{S}(V)} dA_{\mathbf{s}} \{I_{\mu\eta}(\mathbf{s}) - I_{\eta\mu}^*(\mathbf{s})\}}{4(\tilde{\omega}_\mu - \tilde{\omega}_\eta^*)(\omega - \tilde{\omega}_\mu)}, \tag{D16}$$

where $I_{\mu\eta} = [\mathbf{n}_{\mathbf{s}} \times \tilde{\mathbf{f}}_\mu(\mathbf{s})]^{\mathrm{t}} \cdot [\nabla_{\mathbf{s}} \times \tilde{\mathbf{f}}_\eta^*(\mathbf{s})]$. The volume term is defined from

$$K_{\mu\eta}^{\mathrm{vol}}(\omega) = \frac{\int_V d\mathbf{s}\, R_{\mu\eta}(\mathbf{s}, \omega) \tilde{\mathbf{f}}_\mu(\mathbf{s}) \cdot \tilde{\mathbf{f}}_\eta^*(\mathbf{s})}{4(\tilde{\omega}_\mu - \tilde{\omega}_\eta^*)(\omega - \tilde{\omega}_\mu)} + M_{\mu\eta}(\omega) \tag{D17}$$

with

$$R_{\mu\eta}(\mathbf{s}, \omega) = \frac{2i\tilde{\omega}_\eta^{*2} \epsilon_I(\mathbf{r}, \tilde{\omega}_\eta^*)(\omega - \tilde{\omega}_\mu)}{\omega - \tilde{\omega}_\eta^*} + \frac{2i\omega^2 \epsilon_I(\mathbf{r}, \omega)(\tilde{\omega}_\mu - \tilde{\omega}_\eta^*)}{\omega - \tilde{\omega}_\eta^*} \tag{D18}$$

and

$$M_{\mu\eta}(\omega) = \sum_j \frac{[\tilde{\Omega}_j^*]^2 \int_V d\mathbf{s}\, \sigma_j(\mathbf{r}) \tilde{\mathbf{f}}_\mu(\mathbf{s}) \cdot \tilde{\mathbf{f}}_\eta^*(\mathbf{s})}{4(\tilde{\Omega}_j^* - \tilde{\omega}_\mu)(\tilde{\Omega}_j^* - \omega)(\tilde{\Omega}_j^* - \tilde{\omega}_\eta^*)}, \tag{D19}$$

which originates from the volume part of the Green's identity.

Taking the subsequent limits of $\sigma_j \to 0$ and $\gamma_\mu \to 0$ (and vanishing QNM functions on the cavity boundary and in the background region), we again recover the usual NM expansion, similar to the one-dimensional case. A formal proof of this limit in combination with a specific inner product of QNMs can be found in Ref. [32].


[1] A. Vyas, V. Rana, D. Gadani, and A. Prajapati, Cavity perturbation technique for complex permittivity measurement of dielectric materials at *x*-band microwave frequency, in *2008 International Conference on Recent Advances in Microwave Theory and Applications* (IEEE, Piscataway, NJ, 2008).

[2] R. Waldron, Perturbation theory of resonant cavities, Proc. IEE Part C: Monographs **107**, 272 (1960).

[3] P. Čičmanec, Cavity perturbation method for measurement of permittivity and conductivity of medium lossy semiconductors and dielectrics, Solid-State Electron. **14**, 153 (1971).

[4] P. Lalanne, W. Yan, K. Vynck, C. Sauvan, and J.-P. Hugonin, Light interaction with photonic and plasmonic resonances, Laser Photon. Rev. **12**, 1700113 (2018).

[5] K. Ujihara, Quantum theory of a one-dimensional laser with output coupling. Linear theory, Phys. Rev. A **16**, 652 (1977).

[6] J. Gea-Banacloche, N. Lu, L. M. Pedrotti, S. Prasad, M. O. Scully, and K. Wódkiewicz, Treatment of the spectrum of squeezing based on the modes of the universe. I. Theory and a physical picture, Phys. Rev. A **41**, 369 (1990).

[7] R. J. Glauber and M. Lewenstein, Quantum optics of dielectric media, Phys. Rev. A **43**, 467 (1991).

[8] B. Huttner and S. M. Barnett, Quantization of the electromagnetic field in dielectrics, Phys. Rev. A **46**, 4306 (1992).

[9] G. S. Agarwal, *Quantum Optics* (Cambridge University Press, Cambridge, 2013).

[10] H. M. Lai, P. T. Leung, K. Young, P. W. Barber, and S. C. Hill, Time-independent perturbation for leaking electromagnetic modes in open systems with application to resonances in microdroplets, Phys. Rev. A **41**, 5187 (1990).

[11] P. T. Leung, S. Y. Liu, and K. Young, Completeness and orthogonality of quasinormal modes in leaky optical cavities, Phys. Rev. A **49**, 3057 (1994).

[12] E. S. C. Ching, P. T. Leung, A. Maassen van den Brink, W. M. Suen, S. S. Tong, and K. Young, Quasinormal-mode expansion for waves in open systems, Rev. Mod. Phys. **70**, 1545 (1998).

[13] P. T. Kristensen, C. Van Vlack, and S. Hughes, Generalized effective mode volume for leaky optical cavities, Opt. Lett. **37**, 1649 (2012).

[14] P. T. Kristensen and S. Hughes, Modes and mode volumes of leaky optical cavities and plasmonic nanoresonators, ACS Photon. **1**, 2 (2014).

[15] P. T. Kristensen, K. Herrmann, F. Intravaia, and K. Busch, Modeling electromagnetic resonators using quasinormal modes, Adv. Opt. Photon. **12**, 612 (2020).

[16] P. T. Leung, S. Y. Liu, and K. Young, Completeness and time-independent perturbation of the quasinormal modes of an absorptive and leaky cavity, Phys. Rev. A **49**, 3982 (1994).

[17] E. A. Muljarov, W. Langbein, and R. Zimmermann, Brillouin-wigner perturbation theory in open electromagnetic systems, Europhys. Lett. **92**, 50010 (2010).

[18] C. Sauvan, J. P. Hugonin, I. S. Maksymov, and P. Lalanne, Theory of the spontaneous optical emission of nanosize photonic and plasmon resonators, Phys. Rev. Lett. **110**, 237401 (2013).

[19] L. Zschiedrich, F. Binkowski, N. Nikolay, O. Benson, G. Kewes, and S. Burger, Riesz-projection-based theory of light-matter interaction in dispersive nanoresonators, Phys. Rev. A **98**, 043806 (2018).

[20] C. Carlson and S. Hughes, Dissipative modes, Purcell factors, and directional beta factors in gold bowtie nanoantenna structures, Phys. Rev. B **102**, 155301 (2020).

[21] F. Binkowski, L. Zschiedrich, M. Hammerschmidt, and S. Burger, Modal analysis for nanoplasmonics with nonlocal material properties, Phys. Rev. B **100**, 155406 (2019).

[22] P. T. Kristensen, J. R. de Lasson, and N. Gregersen, Calculation, normalization, and perturbation of quasinormal modes in coupled cavity-waveguide systems, Opt. Lett. **39**, 6359 (2014).

[23] J. R. Capers, D. A. Patient, and S. A. R. Horsley, Inverse design in the complex plane: Manipulating quasinormal modes, Phys. Rev. A **106**, 053523 (2022).

[24] J. Yang, H. Giessen, and P. Lalanne, Simple analytical expression for the peak-frequency shifts of plasmonic resonances for sensing, Nano Lett. **15**, 3439 (2015).

[25] K. G. Cognée, W. Yan, F. L. China, D. Balestri, F. Intonti, M. Gurioli, A. F. Koenderink, and P. Lalanne, Mapping complex mode volumes with cavity perturbation theory, Optica **6**, 269 (2019).

[26] T. Christopoulos, O. Tsilipakos, and E. E. Kriezis, Perturbation theory for kerr nonlinear leaky cavities, Opt. Lett. **45**, 6442 (2020).

[27] J. Ren, S. Franke, and S. Hughes, Quasinormal modes, local density of states, and classical purcell factors for coupled loss-gain resonators, Phys. Rev. X **11**, 041020 (2021).

[28] R.-C. Ge, P. T. Kristensen, J. F. Young, and S. Hughes, Quasinormal mode approach to modelling light-emission and propagation in nanoplasmonics, New J. Phys. **16**, 113048 (2014).

[29] M. Kamandar Dezfouli and S. Hughes, Regularized quasinormal modes for plasmonic resonators and open cavities, Phys. Rev. B **97**, 115302 (2018).

[30] F. Binkowski, F. Betz, R. Colom, M. Hammerschmidt, L. Zschiedrich, and S. Burger, Quasinormal mode expansion of optical far-field quantities, Phys. Rev. B **102**, 035432 (2020).

[31] S. Franke, S. Hughes, M. K. Dezfouli, P. T. Kristensen, K. Busch, A. Knorr, and M. Richter, Quantization of quasinormal modes for open cavities and plasmonic cavity quantum electrodynamics, Phys. Rev. Lett. **122**, 213901 (2019).

[32] S. Franke, J. Ren, S. Hughes, and M. Richter, Fluctuation-dissipation theorem and fundamental photon commutation relations in lossy nanostructures using quasinormal modes, Phys. Rev. Res. **2**, 033332 (2020).

[33] J. Ren, S. Franke, A. Knorr, M. Richter, and S. Hughes, Near-field to far-field transformations of optical quasinormal modes and efficient calculation of quantized quasinormal modes for open cavities and plasmonic resonators, Phys. Rev. B **101**, 205402 (2020).

[34] Y. Yu, A. M. Delgoffe, A. Miranda, A. Lyasota, B. Dwir, A. Rudra, and E. Kapon, Remote excitation between quantum emitters mediated by an optical fano resonance, Optica **8**, 1605 (2021).

[35] M. Richter and S. Hughes, Enhanced TEMPO algorithm for quantum path integrals with off-diagonal system-bath coupling: Applications to photonic quantum networks, Phys. Rev. Lett. **128**, 167403 (2022).

[36] P. Leung, S. Tong, and K. Young, Two-component eigenfunction expansion for open systems described by the wave equation I: Completeness of expansion, J. Phys. A: Math. Gen. **30**, 2139 (1997).

[37] K. M. Lee, P. T. Leung, and K. M. Pang, Dyadic formulation of morphology-dependent resonances. I. Completeness relation, J. Opt. Soc. Am. B **16**, 1409 (1999).

[38] B. Vial, F. Zolla, A. Nicolet, and M. Commandré, Quasimodal expansion of electromagnetic fields in open two-dimensional structures, Phys. Rev. A **89**, 023829 (2014).

[39] W. Yan, R. Faggiani, and P. Lalanne, Rigorous modal analysis of plasmonic nanoresonators, Phys. Rev. B **97**, 205422 (2018).

[40] S. Franke, J. Ren, M. Richter, A. Knorr, and S. Hughes, Fermi's golden rule for spontaneous emission in absorptive and amplifying media, Phys. Rev. Lett. **127**, 013602 (2021).

[41] S. Franke, J. Ren, and S. Hughes, Quantized quasinormal-mode theory of coupled lossy and amplifying resonators, Phys. Rev. A **105**, 023702 (2022).

[42] S. Schelkunoff, Some equivalence theorems of electromagnetics and their application to radiation problems, Bell Syst. Tech. J. **15**, 92 (1936).

[43] P. T. Leung, S. Y. Liu, S. S. Tong, and K. Young, Time-independent perturbation theory for quasinormal modes in leaky optical cavities, Phys. Rev. A **49**, 3068 (1994).

[44] A. Settimi, S. Severini, N. Mattiucci, C. Sibilia, M. Centini, G. D'Aguanno, M. Bertolotti, M. Scalora, M. Bloemer, and C. M. Bowden, Quasinormal-mode description of waves in one-dimensional photonic crystals, Phys. Rev. E **68**, 026614 (2003).

[45] M. Maksimovic, M. Hammer, and E. van Groesen, Coupled optical defect microcavities in 1D photonic crystals and quasi-normal modes, in *Integrated Optics: Devices, Materials, and Technologies XII*, Vol. 6896, edited by C. M. Greiner and C. A. Waechter (International Society for Optics and Photonics, Bellingham, WA, 2008), pp. 23–34.

[46] F. Johansson *et al.*, MPMATH: A Python library for arbitrary-precision floating-point arithmetic (version 0.18) (2013), `http://mpmath.org/`.

[47] N. A. Gippius, T. Weiss, S. G. Tikhodeev, and H. Giessen, Resonant mode coupling of optical resonances in stacked nanostructures, Opt. Express **18**, 7569 (2010).

[48] S. G. Johnson, M. L. Povinelli, M. Soljačić, A. Karalis, S. Jacobs, and J. D. Joannopoulos, Roughness losses and volume-current methods in photonic-crystal waveguides, Appl. Phys. B **81**, 283 (2005).

[49] L. Ramunno and S. Hughes, Disorder-induced resonance shifts in high-index-contrast photonic crystal nanocavities, Phys. Rev. B **79**, 161303(R) (2009).

[50] Q. Bai, M. Perrin, C. Sauvan, J.-P. Hugonin, and P. Lalanne, Efficient and intuitive method for the analysis of light scattering by a resonant nanostructure, Opt. Express **21**, 27371 (2013).

[51] COMSOL Inc., COMSOL multiphysics v 5.4.

[52] J. R. de Lasson, P. T. Kristensen, J. Mørk, and N. Gregersen, Semianalytical quasi-normal mode theory for the local density

of states in coupled photonic crystal cavity-waveguide structures, Opt. Lett. **40**, 5790 (2015).

[53] M. Kamandar Dezfouli, R. Gordon, and S. Hughes, Modal theory of modified spontaneous emission for a hybrid plasmonic photonic-crystal cavity system, Phys. Rev. A **95**, 013846 (2017).

[54] A.-W. El-Sayed and S. Hughes, Quasinormal-mode theory of elastic Purcell factors and Fano resonances of optomechanical beams, Phys. Rev. Res. **2**, 043290 (2020).

[55] J. Ren, S. Franke, and S. Hughes, Quasinormal mode theory of chiral power flow from linearly polarized dipole emitters coupled to index-modulated microring resonators close to an exceptional point, ACS Photon. **9**, 1315 (2022).

[56] P. T. Kristensen, J. R. de Lasson, M. Heuck, N. Gregersen, and J. Mørk, On the theory of coupled modes in optical cavity-waveguide structures, J. Lightwave Technol. **35**, 4247 (2017).

[57] K. C. Ho, P. T. Leung, A. Maassen van den Brink, and K. Young, Second quantization of open systems using quasinormal modes, Phys. Rev. E **58**, 2965 (1998).

[58] S. Franke, M. Richter, J. Ren, A. Knorr, and S. Hughes, Quantized quasinormal-mode description of nonlinear cavity-QED effects from coupled resonators with a Fano-like resonance, Phys. Rev. Res. **2**, 033456 (2020).

[59] J. Ren, S. Franke, and S. Hughes, Connecting classical and quantum mode theories for coupled lossy cavity resonators using quasinormal modes, ACS Photon. **9**, 138 (2022).

[60] H. T. Dung, L. Knöll, and D.-G. Welsch, Spontaneous decay in the presence of dispersing and absorbing bodies: General theory and application to a spherical cavity, Phys. Rev. A **62**, 053804 (2000).

[61] R.-C. Ge and S. Hughes, Quantum dynamics of two quantum dots coupled through localized plasmons: An intuitive and accurate quantum optics approach using quasinormal modes, Phys. Rev. B **92**, 205420 (2015).

[62] J. P. Clemens, L. Horvath, B. C. Sanders, and H. J. Carmichael, Collective spontaneous emission from a line of atoms, Phys. Rev. A **68**, 023809 (2003).

[63] J. Clemens, L. Horvath, B. C. Sanders, and H. Carmichael, Shot-to-shot fluctuations in the directed superradiant emission from extended atomic samples, J. Opt. B: Quantum Semiclassical Opt. **6**, S736 (2004).

[64] J. S. Toll, Causality and the dispersion relation: Logical foundations, Phys. Rev. **104**, 1760 (1956).

[65] L. D. Landau, J. Bell, M. Kearsley, L. Pitaevskii, E. Lifshitz, and J. Sykes, *Electrodynamics of Continuous Media*, Vol. 8 (Elsevier, Amsterdam, 2013).